Design and Synthesis of Amino-Acids derived AIE active systems and their applications

M.Sc. Thesis

By Reetik Chib



DEPARTMENT OF CHEMISTRY INDIAN INSTITUTE OF TECHNOLOGY INDORE

May 2025

Design and Synthesis of Amino-Acids derived AIE active systems and their applications

A THESIS

Submitted in partial fulfilment of the requirements for the award of the degree

of

Master of Science

by

Reetik Chib



DEPARTMENT OF CHEMISTRY INDIAN INSTITUTE OF TECHNOLOGY INDORE

May 2025



Indian Institute of Technology Indore

CANDIDATE'S DECLARATION

I hereby certify that the work which is being presented in the thesis entitled 'Design and Synthesis of Amino acids derived AIE active systems and their applications' in the partial fulfilment of the requirements for the award of the degree of MASTER OF SCIENCE and submitted in the DEPARTMENT OF CHEMISTRY, Indian Institute of Technology Indore, is an authentic record of my own work carried out during the time period from July 2024 to May 2025 under the supervision of Dr. Tridib Kumar Sarma, Discipline of Chemistry, IIT Indore.

The matter presented in this thesis has not been submitted by me for the award of any other degree of this or any other institute.

Signature of the student Date: 20/05/2025 (REETIK CHIB)

This is to certify that the above statement made by the candidate is correct to the best of my knowledge.

Signature of the Supervisor

(Dr.Tridib Kumar Sarma)

Reetik Chib has successfully given his M.Sc. Oral Examination held on 15th May 2025.

Signature of Supervisor of MSc thesis

Date: 20/05/2025

ACKNOWLEDGEMENT

I would like to express my deepest gratitude to my supervisor, **Dr. Tridib Kumar Sarma**, for his invaluable guidance, support, and constant encouragement throughout the course of this research project. His scientific insight, enthusiasm for research, and dedication to mentoring have been a continuous source of inspiration for me.

I am also profoundly thankful to the **Department of Chemistry, IIT Indore**, for providing me the opportunity to undertake my **M.Sc. Research Project Stage-II** in such a dynamic and intellectually stimulating environment. I extend my sincere appreciation to **Prof. Tushar Kanti Mukherjee**, Head of the Department of Chemistry, for his leadership and support.

I gratefully acknowledge the **technical staff at the Sophisticated**Instrumentation Centre (SIC), IIT Indore, for their assistance with instrumental analyses, which were crucial to the progress of my work.

My heartfelt thanks go to my mentor, Mr. Ravindra Vishwakarma, for his consistent guidance, encouragement, and generous nature, which have greatly contributed to my learning and growth.

I am also thankful to my **lab seniors**, whose experience, timely suggestions, and willingness to help have played a significant role in shaping both the technical and practical aspects of my work.

I would also like to sincerely thank **all my lab mates**, whose help, camaraderie, and collaborative spirit made this journey smooth and enjoyable.

Lastly, I extend my heartfelt gratitude to my **family**, **close friends**, and **those who stood by me throughout this journey**, offering constant emotional support and understanding, both in moments of challenge and success.

Reetik Chib
(M.Sc. Student)

TABLE OF CONTENTS

>	List of Figure	II
>	List of Tables	V
>	Abbreviations	VI
>	Abstract	VII
>	Chapter 1: Introduction	1
>	1.1. What is AIE?	2
	1.2. Applications of AIE active systems	3
>	1.3. Coacervation driven emission arising from	6
	LLPS	
>	1.4. Self-assembly of Amino Acids	9
>	Chapter 2: Motivation	11
>	Chapter 3: Objective	13
>	Chapter 4: Experimental Details	14
	4.1. Materials and Methods	14
	4.2. Synthesis of L-ArgPy	14
>	Chapter 5: Results and Discussions	
>	5.1. Characterization of L-ArgPy	16
	5.2. Photophysical Properties	19
	5.3. TCSPC study	22
	5.4. Quantum Yield Calculation	24
>	5.5. Morphological and Mechanistic Study	25
>	Chapter 6: Dual Emissive nature of L-ArgPy	33
>	Chapter 7: Future Scope of Work	38
>	Chapter 8: Conclusion	39
	Chanter 9. References	<i>Δ</i> 1

LIST OF FIGURES

- **Figure 1.** Simplified Jablonski diagram of the photophysical processes in singlet (left) and triplet (right) states. (Abbreviations: A: absorption; DF: delayed fluorescence; F: fluorescence; IC: internal conversion; ISC: intersystem crossing; P: phosphorescence; RISC: reverse intersystem crossing and VR: vibrational relaxation².
- Figure 2. Difference between non-emissive and emissive in aggregation³.
- **Figure 3.** Biomedical Applications of AIEgens².
- **Figure 4.** a) Proposed mechanism of molecular arrangement upon temperature change, b) Fluorescence images of the thermos-responsive polymer under UV light at 30 °C, 40 °C, and 50 °C, respectively, c) Fluorescence intensity plot of the polymer at 30 °C, 40 °C, and 50 °C¹⁴
- Figure 5. Mechanistic insight into dual peaks⁵.
- Figure 6. Application of Dual-emission ratio-metric FL probes¹¹.
- Figure 7. Process of liquid-liquid phase separation¹⁸.
- **Figure 8.** Schematic illustration of coacervation-induced emission (CIE) using AIEgen–peptide conjugates²¹.
- **Figure 9.** Schematic representation of the proposed synthetic approach employing coacervate droplets, formed via bioinspired liquid—liquid phase separation (LLPS), as a metastable dormant reservoir of monomers to enable controlled supramolecular polymerization²⁴.
- **Figure 10.** Amino acids, the basic units of proteinaceous biomolecules, can assemble into various nanostructures with diverse applications in bioinspired nanotechnology and biomedical applications²⁹.
- **Figure 11.** Anti-bacterial properties of the TGP-nano aggregates and their respective structural similarities with Arginine³³.
- Figure 12. FT-IR spectra of L-ArgPy.
- Figure 13. LC-MS data of L-ArgPy.
- Figure 14. ¹H NMR spectra of L-ArgPy in DMSO-d₆.

Figure 15. a) Photographs of the AIE activity, b) UV-visible spectrum, and c. FL intensity spectrum (λ_{Exc} =365 nm) of the L-ArgPy in DMSO-Water mixture.

Fig. 16. a) Photographs of the AIE activity, b) UV-visible spectrum, and c) FL intensity spectrum (λ_{Exc} =365 nm) of the L-ArgPy in MeOH-Water mixture.

Figure 17. TCSPC graph of L-ArgPy when aggregated with MeOH-H₂0 mixture.

Figure 18. a) LLPS behavior of L-ArgPy in a MeOH–water mixture (90% v/v) upon aggregation, **b)** FE-SEM image of L-ArgPy in MeOH–water (90% v/v) taken after 40 hours, **c)** Confocal image of L-ArgPy in MeOH–water (90% v/v) captured after 24 hours.

Figure 19. a) Hydrodynamic diameter and particle size distribution of the L-ArgPy in a MeOH-water mixture (10:90 v/v), (20ul from a 1mg/ml mixture). **B)** Zeta potential of the L-ArgPy aggregated at fw =0 and 90% in MeOH-H2O mixture (at pH 4,7 and 10, respectively).

Figure 20. a) Proposed mechanism of aggregation of L-ArgPy in a MeOH–water mixture (90% v/v water). **b)** Confocal microscopy images of L-ArgPy recorded at different time intervals - 12 h, 24 h, and 40 h-show the progression of aggregation and morphological evolution.

Figure 21 a) UV–Visible absorption spectra of L-ArgPy in MeOH after aggregation with 90% (v/v) water at different pH conditions -acidic (pH 4), neutral (pH 7), and basic (pH 9), along with a schematic representation of the proposed aggregation mechanism under these pH environments. **b)** Confocal microscopy images of L-ArgPy under basic, neutral, and acidic conditions, respectively.

Figure 22. a) DLS profile of L-ArgPy in a DMSO-water mixture (90% v/v), **b)** Zeta potential measurements of L-ArgPy in DMSO-water (90% v/v), ATP, and the L-ArgPy + ATP complex, **c)** Confocal image of L-ArgPy in DMSO-water (90% v/v) acquired 12 hours post-aggregation.

Figure 23. Schematic representation of the proposed synthetic approach, where coacervate droplets are formed via liquid–liquid phase

separation (LLPS) of L-ArgPy, enabling controlled supramolecular polymerization.

Figure 24. a) FL intensity spectrum (λ_{Exc} =365nm), **b)** Photographs (under UV light) of L-ArgPy in various solvents, **c)** FL (solid-state) intensity spectrum of the L-ArgPy and **d)** Photograph of L-ArgPy under UV light.

Figure 25. a) Emission spectrum of L-ArgPy in MeOH at different excitation wavelengths (290 nm,365 nm, and 400 nm), respectively, **b)** 3-D spectra (contour view) of L-ArgPy in MeOH.

Figure 26. The emission spectrum of L-ArgPy in MeOH-Water (50% v/v) at different excitation wavelengths (290 nm,365 nm, and 400 nm), respectively.

Figure. 27. TCSPC study of L-ArgPy in MeOH and CAN.

LIST OF TABLES

Table 1. TCSPC Table of L-ArgPy when aggregated with MeOH-H₂0 mixture

Table 2. For quantum yield, and radiative, non-radiative, and electron transfer rate constant of L-ArgPy in MeOH-H₂O mixture.

Table 3. TCSPC Table of L-ArgPy in MeOH and ACN.

ABBREVIATIONS

nm nanometer

cm centimeter

Fl. intensity Fluorescence Intensity

NMR Nuclear Magnetic Resonance

LC-MS Liquid Chromatography Mass

Spectrometry

FT-IR Fourier-transform infrared

spectroscopy

AIE Aggregation-Induced Emissions

ACQ Aggregation-Caused Quenching

CIE Coacervation-Induced Emissions

UV-Vis Ultraviolet-Visible spectroscopy

Spectroscopy

TCSPC Time-related single photon counting

LLPS Liquid-Liquid phase transition

LST Liquid to Solid transformation

Abstract

Aggregation-induced emission (AIE) materials have garnered significant attention due to their unique photophysical properties and broad potential in sensing and bioimaging. In this study, we report the synthesis of an AIE-active Schiff base, L-ArgPy, obtained via a condensation reaction between L-arginine (L-Arg) and 1pyrenecarboxaldehyde (1-PyC). The AIE behaviour of L-ArgPy is attributed to a photoinduced electron transfer (PET) mechanism. Morphological analysis performed using confocal laser scanning microscopy (CLSM) and field-emission scanning electron microscopy (FE-SEM) reveals the formation of well-defined rod-like aggregates in a methanol-water mixture at $f_w = 90\%$ water fraction. A rod-like structure is formed through liquid-liquid phase separation (LLPS), resembling coacervate-like assemblies. The self-assembly is primarily driven by noncovalent interactions, including hydrogen bonding, π – π stacking, and solvent-solute interactions. The unique combination of AIE activity and LLPS-driven morphology makes L-ArgPy a promising candidate for applications in materials science and biomedical fields.

Chapter 1: Introduction

In biological environments, fluorescent imaging has become indispensable for studying live cells, pathogens, and biomolecular interactions. However, traditional fluorophores often face a critical drawback: aggregation-caused quenching (ACQ). In aqueous or crowded media, fluorophores tend to aggregate due to hydrophobic interactions, which activate non-radiative decay pathways and suppress emission¹. Interestingly, this very quenching behaviour can be harnessed as a functional signal in fluorescence-based assays, particularly when using aggregation-induced emission (AIE) luminogens, also known as AIEgens.

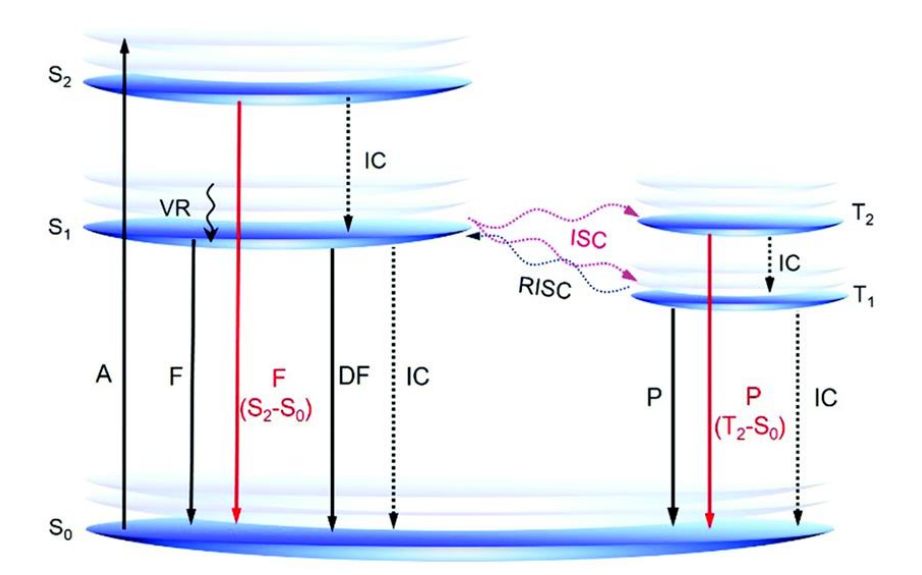


Figure 1. Simplified Jablonski diagram of the photophysical processes in singlet (left) and triplet (right) states. (Abbreviations: A: absorption; DF: delayed fluorescence; F: fluorescence; IC: internal conversion; ISC: intersystem crossing; P: phosphorescence; RISC: reverse intersystem crossing and VR: vibrational relaxation².

At the photophysical level, fluorescence refers to the emission of light by a substance that has absorbed photons, typically from the ultraviolet or visible range³. This process involves transitions between singlet electronic states and is well-represented in a Jablonski diagram, which illustrates pathways such as absorption, internal conversion, intersystem crossing, and fluorescence emission⁴.

1.1. What is Aggregation-Induced Emission (AIE)?

The Jablonski diagram also emphasizes the significance of non-radiative transitions, critical to ACQ and AIE phenomena. Understanding these transitions is vital for designing new materials that efficiently utilize radiative pathways while minimizing non-radiative losses. The initial AIE active molecule, MPPS, exhibits AIE activity in an aggregated state. Aggregation happens by the π , π -stacking phenomenon that occurs amongst the aromatic groups of the individual

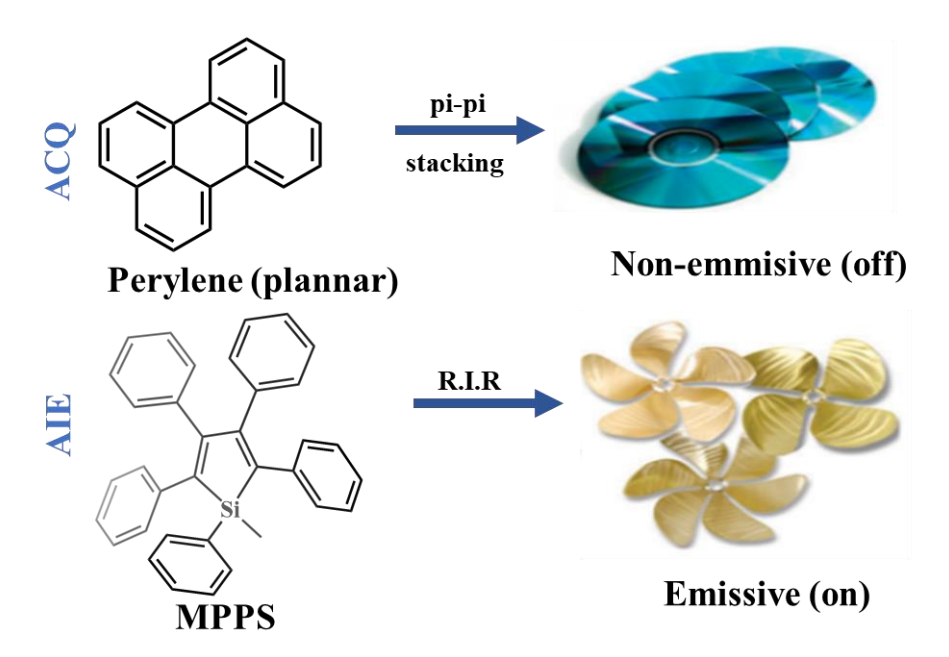


Figure 2. Difference between non-emissive and emissive in aggregation³.

molecules⁵. This stacking effectively limits the free rotation of these groups and consequently restricts the intramolecular motion (RIM). When RIM occurs, the non-radiative transition becomes impeded, leading to the manifestation of fluorescence in the molecules. Unlike classical dyes, AIE-active molecules are weakly or non-emissive in dilute solutions due to active intramolecular rotations or vibrations but become highly luminescent when aggregated⁶. Upon interaction with biological entities such as bacteria or cell membranes, these molecules often form aggregates or undergo conformational locking, thereby

triggering a strong fluorescence signal. This "light-up" behaviour enables high-contrast imaging and has been successfully applied in microbial detection, cancer diagnostics, and organelle-specific staining⁷.

1.2. Applications of AIE active systems

aggregation-induced emission (AIE) concept has transformed the understanding of traditional photophysical phenomena and opened new opportunities in biological analysis, process monitoring, and disease studies⁸. AIE luminogens (AIEgens), weakly or non-emissive as individual molecules but highly fluorescent in aggregates or solid states, offer critical advantages like high brightness, significant Stokes shifts, excellent photostability, and good biocompatibility⁹. These features have made AIEgens valuable for biomedical applications, including sensing biomolecules, cell imaging, in vivo imaging, and cancer theranostics 10. This review summarizes AIE's development in biomedicine, highlights key research directions, and explores the future potential, suggesting that AIEgen-based probes will continue advancing life science and healthcare innovations².

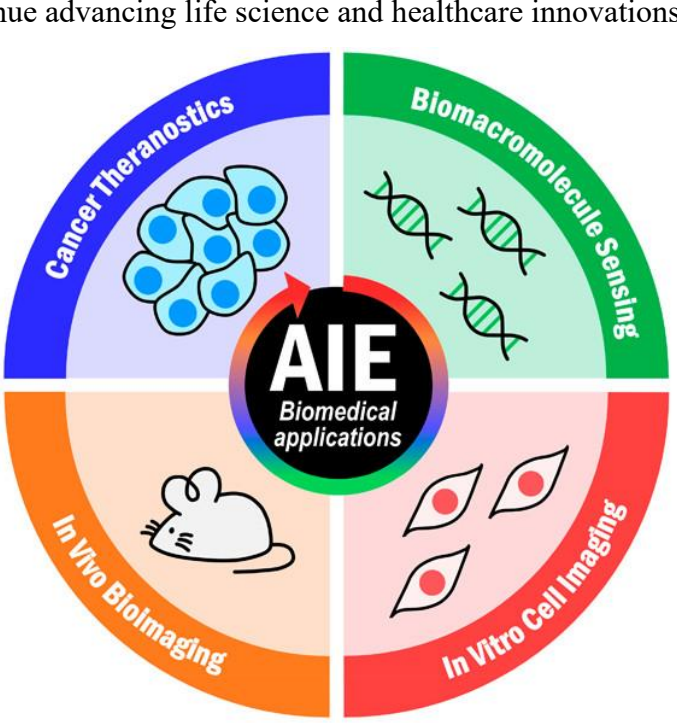


Figure 3. Biomedical Applications of AIEgens².

Beyond RIM (restriction in intermolecular rotation), AIE can manifest through various mechanisms: Coacervation-Induced Emission (CIE) involves fluorescence activation during liquid—liquid phase separation; Crystallization-Induced Enhanced Emission (CIEE) arises from ordered molecular packing in crystalline states; Dual Emission systems display simultaneous monomer and excimer emissions; Crosslink-Enhanced Emission (CEE) results from covalent or non-covalent crosslinking that restricts molecular motions; and Electrochemiluminescence (ECL) combines electrochemical reactions with AIE properties¹⁰. These diverse pathways underscore the versatility of AIE-active materials in applications ranging from bioimaging to optoelectronics.

Dual-emission properties in aggregation-induced emission (AIE) systems arise from the ability of a single molecule to exhibit two distinct emissive states under specific conditions. This behavior is typically influenced by intramolecular charge transfer (ICT), excimer formation, or interactions such as hydrogen bonding and π – π stacking¹¹. In such systems, one emissive state often corresponds to monomeric emission, while the other is attributed to aggregated species or dimer formation. Dual emission is particularly useful in biosensing, enabling precise detection of changes in cellular environments by analyzing emission intensity ratios. Systems using AIE-active nanogels have demonstrated potential for monitoring dynamic processes such as temperature-induced phase transitions¹².

AIE systems with integrated thermo-responsive polymers combine high sensitivity with versatility. The system's ability to transition between hydrophilic and hydrophobic states extends its use to diverse applications, including biomedical imaging and therapeutic monitoring. The correlation between the intensity ratio of the two emissions and the temperature provides a quantitative approach for highly sensitive thermal sensing in biological and environmental systems⁴. In these systems, thermo-responsive polymers undergo a hydrophilic-to-hydrophobic transition as the temperature crosses the

lower critical solution temperature (LCST)¹³. This transition changes the local environment of the AIE luminogenic, causing a spectral shift between two emission states.

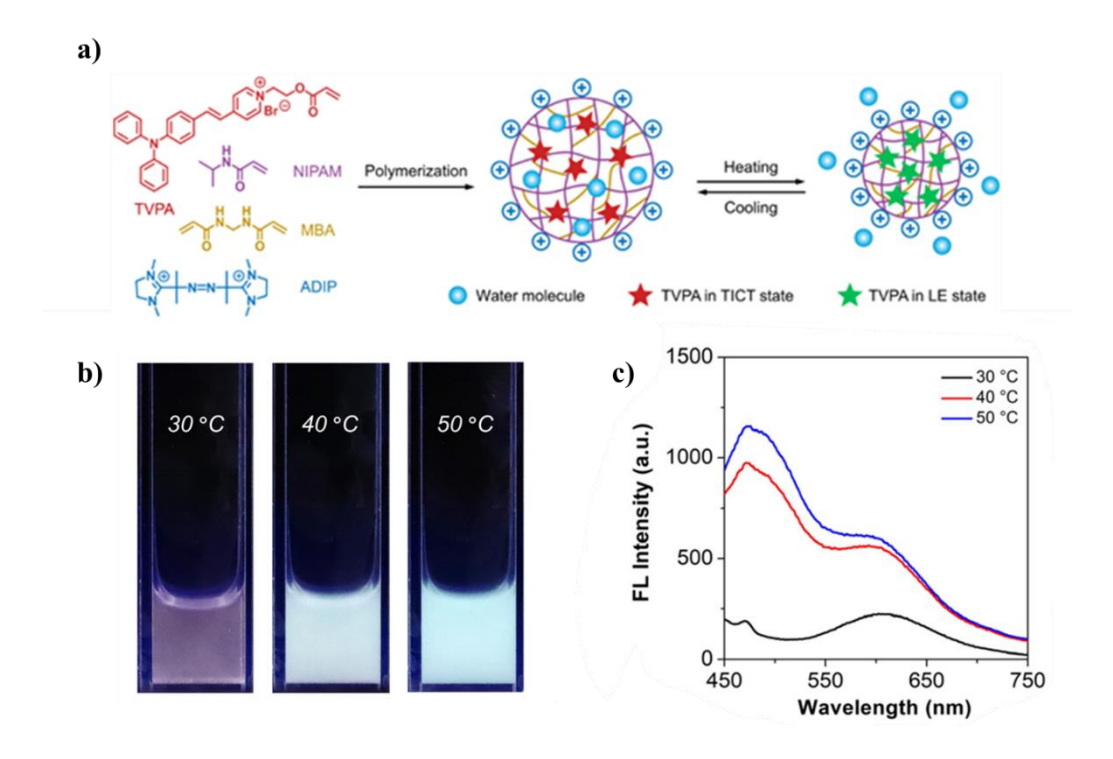


Figure 4. a) Proposed mechanism of molecular arrangement upon temperature change, b) Fluorescence images of the thermos-responsive polymer under UV light at 30 °C, 40 °C, and 50 °C, respectively, c) luorescence intensity plot of the polymer at 30 °C, 40 °C, and 50 °C¹⁴.

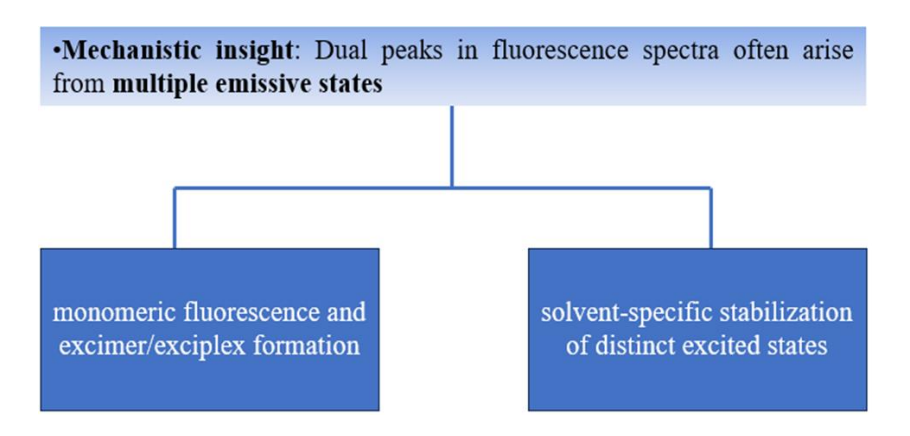


Figure 5. Mechanistic insight into dual peaks⁵.

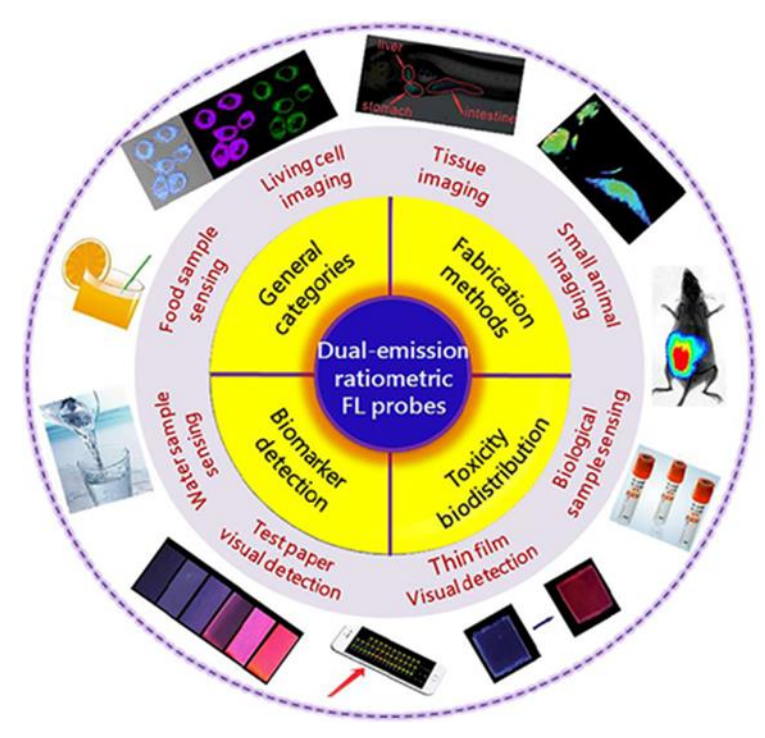


Figure 6. Application of Dual-emission ratio-metric FL probes¹¹.

The diagram shows that external stimuli, such as changes in solvent polarity, pH, or temperature, can strategically modulate dual emission¹⁵. This tunable behaviour makes dual-emissive AIE systems highly versatile for ratio-metric sensing, environmental monitoring, and bioimaging applications, as they provide enhanced precision and sensitivity by leveraging the intensity ratio of the two emissions¹⁶.

1.3. Coacervation-Driven Emission Arising from Liquid-Liquid Phase Separation

Liquid–Liquid Phase Separation (LLPS) is a fundamental process by which a homogeneous solution of macromolecules separates into two immiscible liquid phases: a dense, biomolecule-rich phase (coacervate) and a surrounding dilute phase. This principle is central to the organization of membraneless organelles in cells, such as stress granules, nucleoli, and P-bodies¹⁷. LLPS is driven by multivalent interactions, including electrostatic attractions, π – π stacking, cation– π interactions, and hydrogen bonding among proteins, peptides, and nucleic acids. These interactions can be finely tuned by environmental

factors such as pH, ionic strength, and temperature. In synthetic systems, LLPS provides a powerful strategy to compartmentalize molecules without membranes, and when combined with functional fluorophores (e.g., AIEgens), allows for dynamic visualization of these assemblies

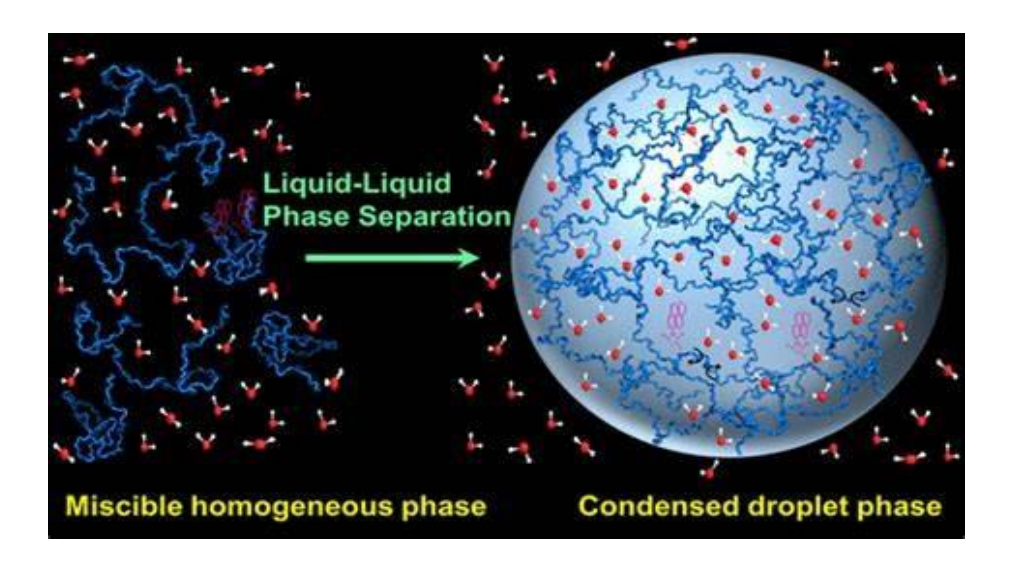


Figure 7. Process of liquid-liquid phase separation¹⁸.

Coacervation-Induced Emission (CIE) is a recently emerging photophysical phenomenon observed in systems that undergo phase separation to form dense coacervates ¹⁹. In many AIE (Aggregation-Induced Emission)-active systems, especially those based on peptide–fluorophore conjugates, the dispersed molecules in dilute aqueous media remain non-emissive due to active intramolecular rotations and weak π – π stacking ⁷. However, upon coacervation—triggered by environmental stimuli such as pH, salt concentration, or molecular crowding—the resulting condensed phase imposes spatial confinement and restricts intramolecular motions (RIM). This restriction activates fluorescence in what was previously a dark state, enabling spatial and temporal tracking of phase-separated domains ²⁰. Such behavior has been used effectively to visualize intracellular condensates and RNA granules using AIE-active fluorophores, as shown by Yang et al. in their design of AIEgen–peptide probes that light up only upon LLPS-induced aggregation

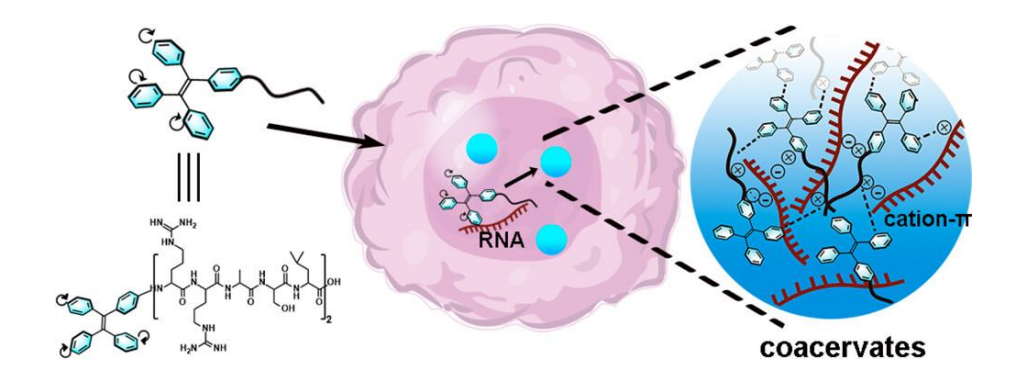


Figure 8. Schematic illustration of coacervation-induced emission (CIE) using AIEgen–peptide conjugates²¹.

Liquid-liquid phase separation (LLPS) is a biophysical phenomenon by which a homogeneous solution of biomolecules separates into two distinct liquid phases, a dense phase (droplets) and a dilute phase, without membrane encapsulation. This process plays a vital role in cellular compartmentalization, forming membraneless organelles such as nucleoli, P-bodies, and stress granules¹⁷. These biomolecular condensates are typically rich in intrinsically disordered proteins (IDPs) and RNA, and they rely on multivalent weak interactions (electrostatic, π - π stacking, hydrogen bonding) to drive dynamic assembly. In parallel, researchers have recently begun integrating AIE and LLPS concepts, giving rise to coacervation-induced emission (CIE) systems, where AIEgens optically report phase separation processes in real time. This integration enables real-time imaging and functional insights into the molecular microenvironment within LLPS droplets, with potential applications in sensing, signal amplification, and synthetic organelle design²².

A milestone in the synthetic mimicry of LLPS came from Patra et al., who reported a naphthalene diimide-based boronic acid derivative (NDBA) capable of pH-triggered phase separation followed by supramolecular polymerization. At mildly basic pH (\sim 9), the molecule undergoes zwitterionic charge balancing, facilitating LLPS through electrostatic interactions and π – π stacking, leading to coacervate droplet

formation²³. These droplets act as metastable reservoirs: initially liquid-like, but over time giving rise to 1D supramolecular fibers, effectively undergoing a liquid-to-solid transition (LST)²⁴. This behavior resembles biological phenomena such as amyloid fibril growth from phase-separated compartments. Their work also demonstrated living supramolecular polymerization, where pre-formed fibers (seeds) could nucleate controlled fiber growth inside the droplets, thereby offering dynamic spatiotemporal control over assembly. This study highlights the utility of LLPS for phase compartmentalization and structural self-assembly, with precise regulation via pH, salt, and time²⁵.

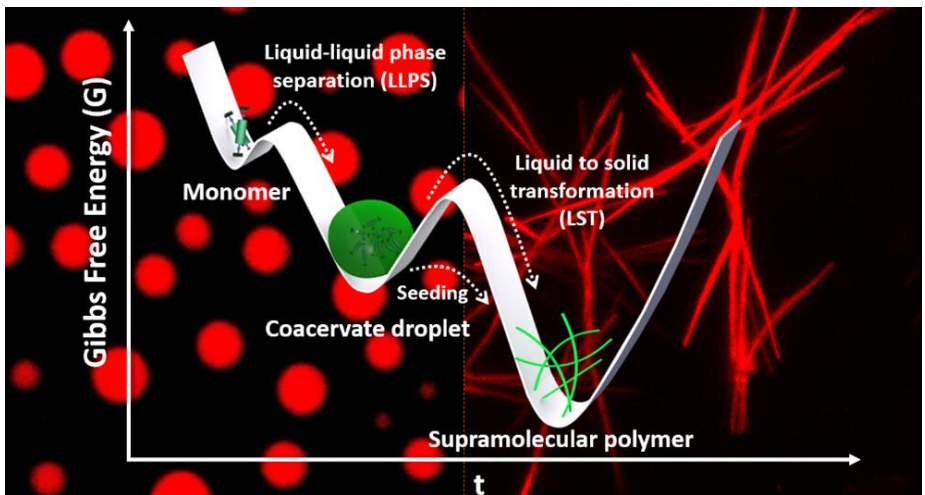


Figure 9. Schematic representation of the proposed synthetic approach employing coacervate droplets, formed via bioinspired liquid–liquid phase separation (LLPS), as a metastable dormant reservoir of monomers to enable controlled supramolecular polymerization²⁴.

1.4. Self-assembly of Amino Acids

Amino acids have a natural ability to self-assemble into well-defined, biocompatible nanostructures²⁶. Amino acids naturally self-assemble into organized structures due to their versatile chemical properties²⁷. On-covalent interactions drive this process. These self-assembled structures, such as nanofibers, sheets, and gels, have potential applications in drug delivery and tissue engineering²⁸. Bioinspired amino acid-based molecules can self-assemble into ordered

nanostructures through noncovalent interactions like hydrogen bonding and π – π stacking. When combined with AIE-active groups, such assemblies often show enhanced fluorescence due to restricted intramolecular motion, enabling real-time monitoring of the aggregation process and offering potential for bioimaging and functional materials²⁹.

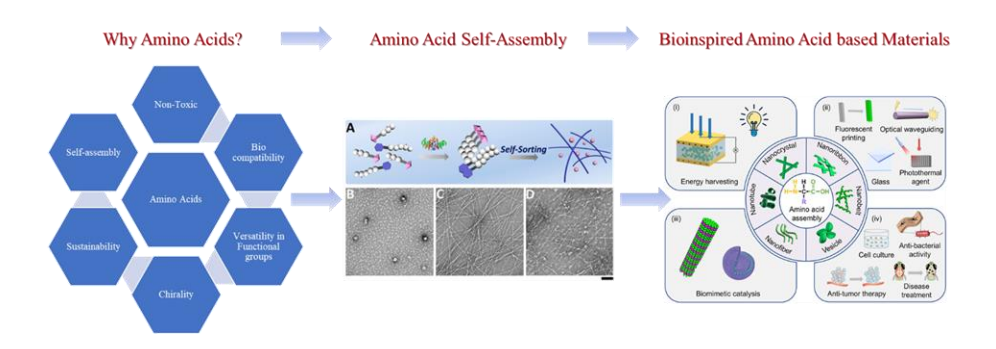


Figure 10. Amino acids, the basic units of proteinaceous biomolecules, can assemble into various nanostructures with diverse applications in bioinspired nanotechnology and biomedical applications²⁹.

Recent studies have focused on AIE-active compounds, particularly those based on Schiff bases, which leverage π - π stacking interactions to limit rotational freedom and enhance light emission³⁰. These compounds hold promise for applications in imaging and sensing, where improved fluorescence can lead to better detection capabilities. This report explores the design and synthesis of Amino acid-based AIE-active compounds, concentrating on structural variations that can optimize their fluorescence properties³¹. By understanding the mechanisms depicted in the Jablonski diagram and leveraging molecular architecture, we wanted to develop materials that demonstrate enhanced emission and serve as practical tools for various applications³².

Chapter 2: Motivation:

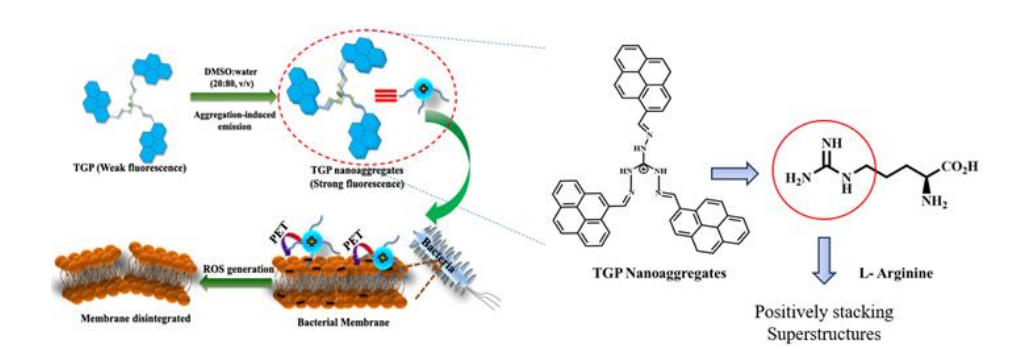


Figure 11. Anti-bacterial properties of the TGP-nano aggregates and their respective structural similarities with Arginine³³.

The potential impact of this research is significant, as it could lead to the development of more effective and versatile AIE-active compounds. I am using the amino acid arginine in my research because it contains a guanidine group. In previous work, TGP nanoaggregates with a guanidine group were synthesized, and they showed effective interactions with cells, making them suitable for bio-sensing³³. Due to its similar structure, Arginine is expected to provide comparable benefits in enhancing cell interaction and sensing capabilities.

Amino acids were used because of the following properties:

- 1. Non-toxic 2. Biocompatibility 3. Versatility
- 4. Chirality 5. Sustainability 6. Self-assembly 12

Their approach elegantly demonstrated how fluorogenic assembly can be achieved through LLPS, combining optical output with phase behavior, and set a precedent for using AIE-active systems to visualize and interrogate condensate dynamics. Building on these foundational works, we developed L-ArgPy, a minimalistic conjugate of pyrene and arginine connected via an imine bond. Our findings reveal that L-ArgPy undergoes pH-sensitive LLPS, likely driven by guanidinium-based electrostatics and pyrene π – π stacking, forming coacervate-like droplets.

Concurrently, L-ArgPy exhibits AIE-like photophysical properties, with fluorescence enhancement and excimer formation observed under conditions promoting phase separation. This system bridges the phase-controlled self-assembly of Patra et al. and the emissive condensate strategy of Yang et al., demonstrating how simple, amino acid–based conjugates can serve as functional models for LLPS-linked emission systems with potential applications in soft matter, imaging, and supramolecular chemistry³⁴.

Chapter 3: Objective:

This study aims to design and synthesize an amino acid-based luminescent compound with potential aggregation-induced emission (AIE) properties. Specifically, the study aims to:

- 1. Synthesize L-ArgPy, a pyrene-carboxaldehyde derivative of arginine, and characterize its structural and optical properties.
- 2. Check the Aggregation-induced emission properties in various solvent mixtures.
- 3. Determine the self-assembled morphology of L-ArgPy in phaseseparated or aggregated states.
- 4. Investigate the mechanism of self-assembly of L-ArgPy at a highly emissive state.
- 5. The possible medicinal significance L-ArgPy and evaluate its antibacterial efficacy against typical microbial strains.
- 6. Investigate the solvent-dependent and dual emission photophysical behaviour of L-ArgPy through fluorescence spectroscopy and time-correlated single-photon counting (TCSPC).

Chapter 4: Experimental Details:

4.1. Materials and Methods:

All reactions were carried out in oven-dried glassware with magnetic stirring. The Bruker AV 500 MHz NMR spectrometer, funded by DST-FIST, Govt. of India, recorded 1 H. Chemical shifts (δ) were measured in ppm (parts per million) using TMS as an internal reference. The Bruker Daltonik High-Performance LC-MS (ESI-TOF) spectrometer was used to obtain high-resolution mass spectra. The Omakar melting point apparatus measures the compounds' melting point. All reagents were used as received from commercial suppliers without further purification. The starting materials were purchased from Sigma-Aldrich with 95-98% purity. The deuterated solvent were brought from TCI with 98-99% purity.

4.2. Synthesis of L-ArgPy:

Chemicals required.

1-Pyrenecarboxaldehyde (1-PyC), L-Arginine (L-Arg), Methanol

Scheme 1

Reaction Conditions:

Yield = 70%

Time = 24 hrs

Temperature = $60 \, ^{\circ}\text{C}$

Under inert atmosphere

Experimental procedure:

1-Pyrenecarboxaldehyde (115.3 mg, 0.5 mmol) and L-arginine (87.1 mg, 0.5 mmol) were dissolved in methanol (15 mL) and stirred in a two-

neck round-bottom flask under a nitrogen atmosphere. The reaction mixture was stirred at 450 rpm and heated to 60 °C in a preheated silicone oil bath for 24 hours. After completion, the mixture was filtered to remove any insoluble material, and the clear filtrate was concentrated using a rotary evaporator. The resulting residue was washed and purified by centrifugation with distilled water and methanol to remove unreacted starting materials and other impurities. The purified product was dried under high vacuum to form the Schiff base conjugate (L-ArgPy), which was then subjected to characterization. **% Yield**: 70%. ¹H NMR (400 MHz, DMSO-D6) d ppm 1.6 (t, 2 H) 2.3 (m, 2 H) 3.2 (s, 1 H) 3.6 (s, 1 H) 4.0 (s, 1 H) 8.1 (s, 1 H) 8.2 (m, 1 H) 8.3 (m, 2 H) 8.5 (d, *J*=7.8 Hz, 1 H) 9.2 (d, *J*=9.3 Hz, 1 H) 9.3 (s, 1H), LCMS (ESI) calculated for [C₂₃H₂₂N₄O₂+H⁺] 387.1816, found 387.2122, ATR-FTIR: $\nu_{(C=N)} = 1623 \text{ cm}^{-1}$.

Chapter 5: Results and Discussions

5.1. Characterization of L-ArgPy:

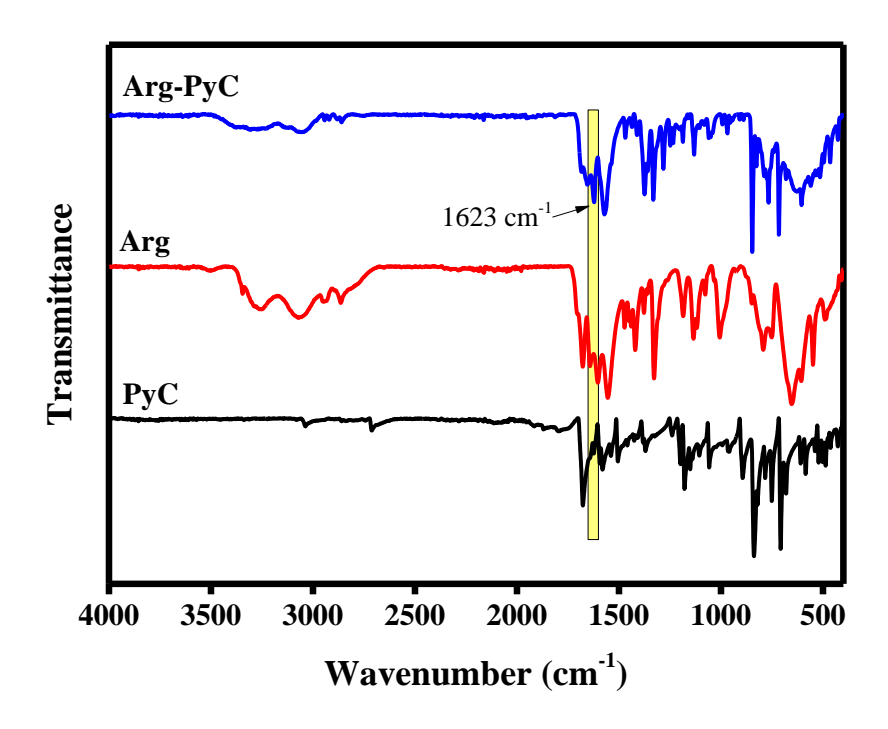


Figure 12. FT-IR spectra of L-ArgPy.

The FTIR spectrum of L-ArgPy confirms the successful formation of the imine bond through Schiff base condensation between pyrene-carboxaldehyde and arginine. A characteristic peak at 1623 cm⁻¹, corresponding to the C=N stretching vibration of the imine group, is observed in the spectrum of L-ArgPy. This peak is absent in the spectra of both precursors, namely pyrene-carboxaldehyde and arginine, indicating the imine bond formation during the reaction. Additionally, the disappearance of the carbonyl stretching peak (~1676 cm¹) from pyrene-carboxaldehyde further validates the condensation reaction. These results confirm the structural integrity of the synthesized compound and the successful completion of the imine formation process.

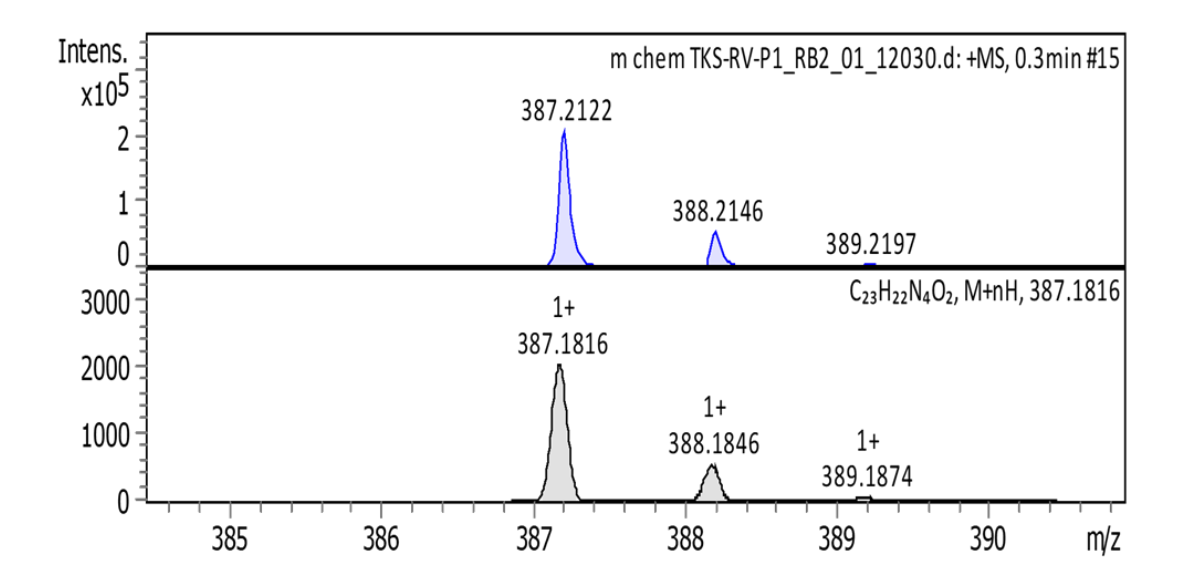


Figure 13. LC-MS data of L-ArgPy.

The mass spectrometry data of L-ArgPy confirms the successful synthesis of the compound. The molecular ion peak at m/z = 387.1816 corresponds to the calculated molecular weight of L-ArgPy, verifying the integrity of the synthesized product. The absence of significant peaks corresponding to precursor fragments further validates the purity of the compound. Additionally, smaller peaks observed in the spectrum may correspond to isotope patterns consistent with the expected mass fragmentation behaviour. These results provide strong evidence for forming L-ArgPy and its structural consistency with the proposed design.

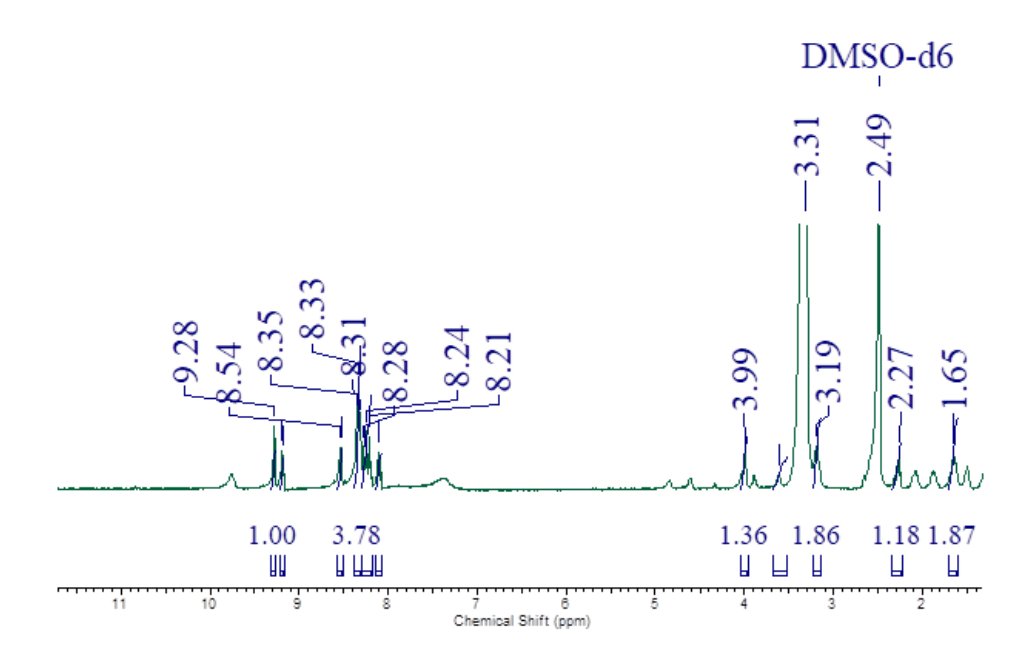


Figure 14. ¹H NMR spectra of L-ArgPy in DMSO-d₆.

The ¹H NMR spectrum of L-ArgPy provides clear evidence for the successful formation of the imine bond. A characteristic singlet appears around 9.28 ppm, corresponding to the proton of the C=N group. The aromatic protons of the pyrene ring are observed in the range of 7.5–8.5 ppm, consistent with its conjugated structure. Additionally, the aliphatic protons of the arginine moiety appear in the region of 1.2–4.0 ppm, confirming the retention of the amino acid framework in the synthesized compound. These spectral features validate the structural integrity of L-ArgPy and confirm the formation of the desired product.

5.2. Photophysical Properties:

S.NO.	DMSO/MeOH (v/v %)	Water (v/v, %)
1.	90	10
2.	80	20
3.	70	30
4.	60	40
5.	50	50
6.	40	60
7.	30	70
8.	20	80
9.	10	90

Aggregation-induced emission (AIE) Activity procedure in Solvent mixtures:

Chemicals required: DMSO/MeOH (HPLC) solvent, HPLC-Water, and L-ArgPy.

Step 1: Took 1 mg of Product 1 dissolved in 1 mL of Methanol/DMSO as a stock solution.

Step 2: Take five vials and a 10 μL sample pipette out from the stock solution and add them to each of the vials. The following solution was prepared:

AIE activity in DMSO-Water Mixture:

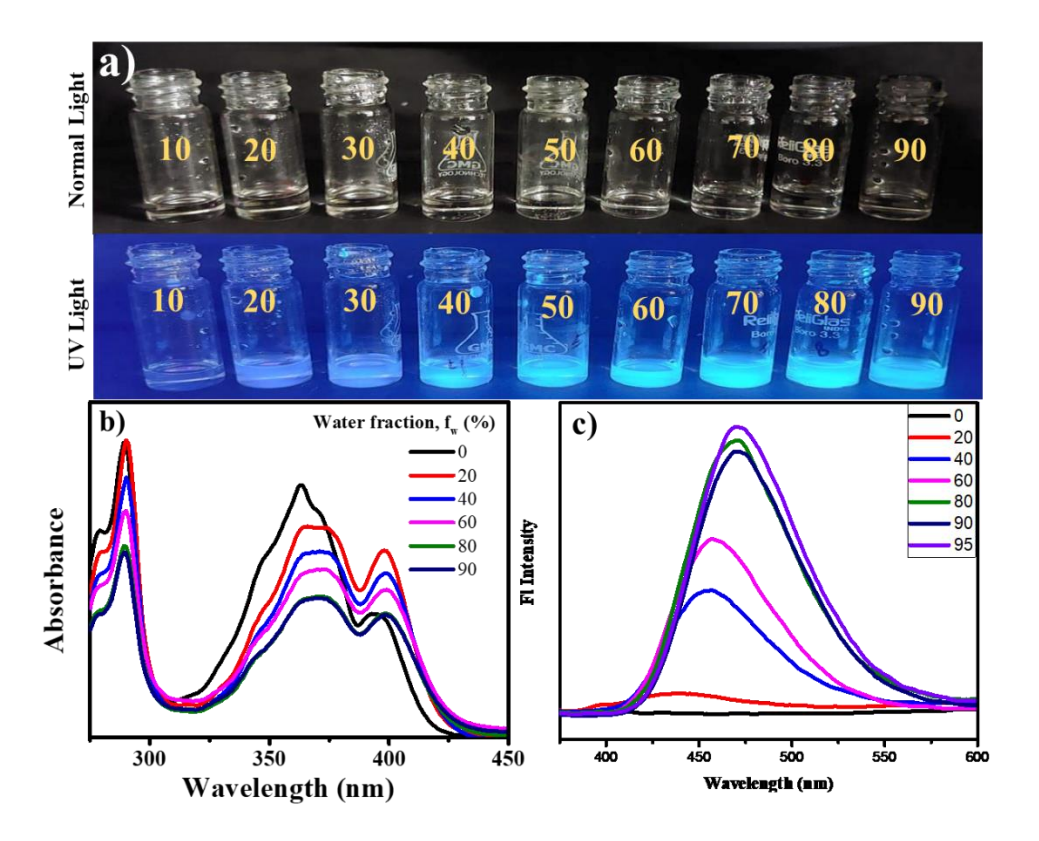


Figure 15. a) Photographs of the AIE activity, b) UV-visible spectrum, and c. FL intensity spectrum (λ_{Exc} =365 nm) of the L-ArgPy in DMSO-Water mixture.

The photophysical properties of L-ArgPy were studied using UV-Visible absorption and fluorescence spectroscopy in various solvent environments. In pure DMSO, the UV-Vis spectrum exhibited absorption bands at 265 nm, 285 nm, 360 nm, and 392 nm (Figure 15b). The bands at 265 nm and 285 nm correspond to higher-energy π - π * transitions (commonly referred to as the second excitonic transition), while the bands at 360 nm and 392 nm are associated with the first excitonic transition of pyrene chromophores, as reported for similar systems in the literature. These transitions are indicative of the possible formation of H-type (blue-shifted, face-to-face stacking) and J-type (red-shifted, head-to-tail stacking) aggregates in pyrene-based assemblies.

Upon increasing the water fraction to fw = 90% in the DMSO- H_2O mixture, a bathochromic shift (red shift) in the absorption bands was

observed, suggesting aggregation due to reduced solubility and enhanced intermolecular interactions in the aqueous environment. Correspondingly, fluorescence measurements revealed that L-ArgPy showed weak intrinsic emission in pure DMSO, which gradually increased with the addition of water, reaching a maximum at fw = 90% (Figure 15a). This enhancement is consistent with aggregation-induced emission (AIE) behavior, where molecular aggregation restricts non-radiative intramolecular motion, leading to radiative decay. However, at fw = 95%, a significant decrease in fluorescence intensity was observed, which is attributed to aggregation-caused quenching (ACQ) resulting from strong π – π stacking interactions between pyrene moieties at high water content³⁵.

AIE activity in MeOH-Water Mixture:

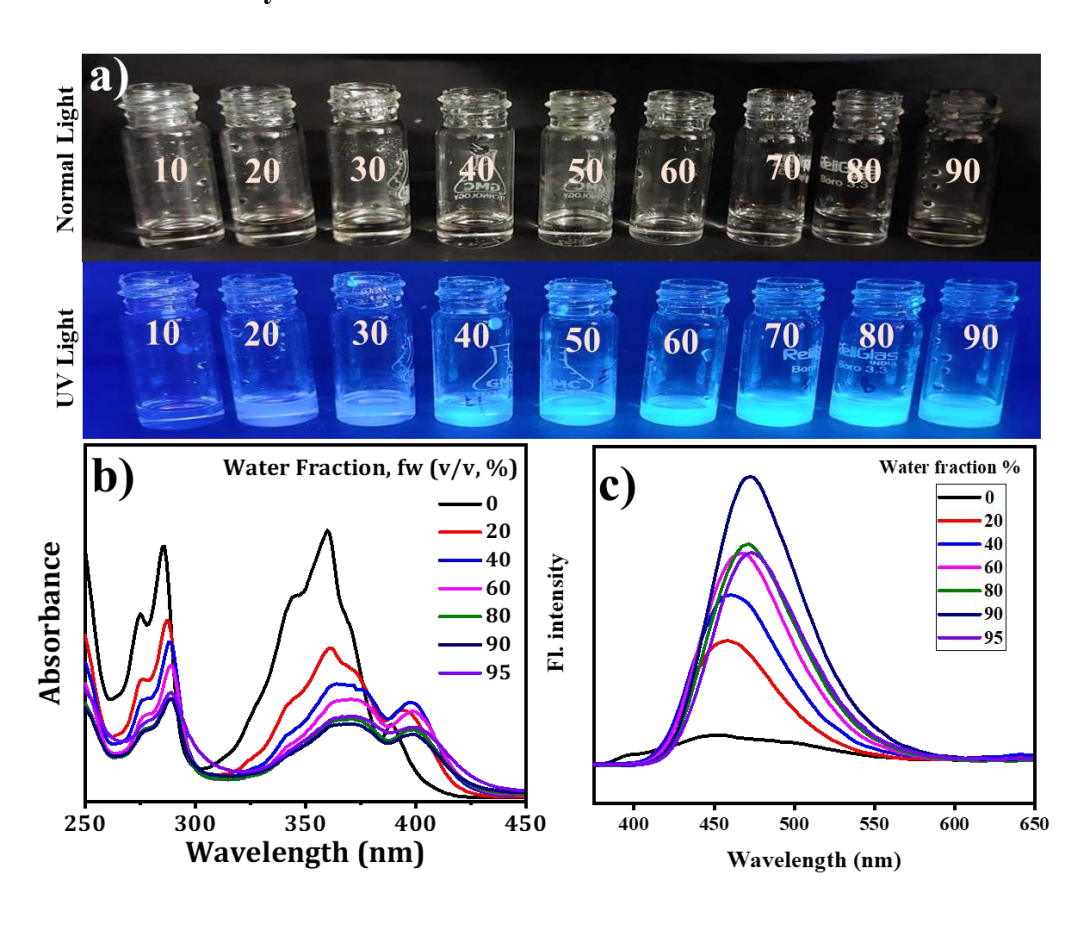


Fig. 16. a) Photographs of the AIE activity, b) UV-visible spectrum, and c) FL intensity spectrum (λ_{Exc} =365 nm) of the L-ArgPy in MeOH-Water mixture.

Additionally, we investigate the AIE activity of L-ArgPy in Methanol-H2O mixture, we got the same pattern in UV- Visible Whereas in pure methanol, the fluorescence was observed at 450 nm and on adding water fraction the red shift and enhancement in intensity was observed at 470 nm (Figure 16 a, b, c).

Furthermore, we investigate the mechanism of AIE activity of L-ArgPy in various solvent mixtures. In the case of DMSO, the emission was observed at 410 nm, whereas when investigated in polar-protic solvent (MeOH), the red shift peak was observed at 450 nm, and with the addition of water, the peak was red-shifted to 470 nm. The red shift in polar and polar protic solvent mixtures is likely associated with photoinduced electron transfer (PET) mechanisms. The aldimine bond of L-ArgPy is isomerized, and after adding water, the isomerization is restricted and inhibits the PET, reducing the non-radiative energy loss and resulting in the enhancement of fluorescence.

5.3. TCSPC (Time correlation single photon count spectroscopy):

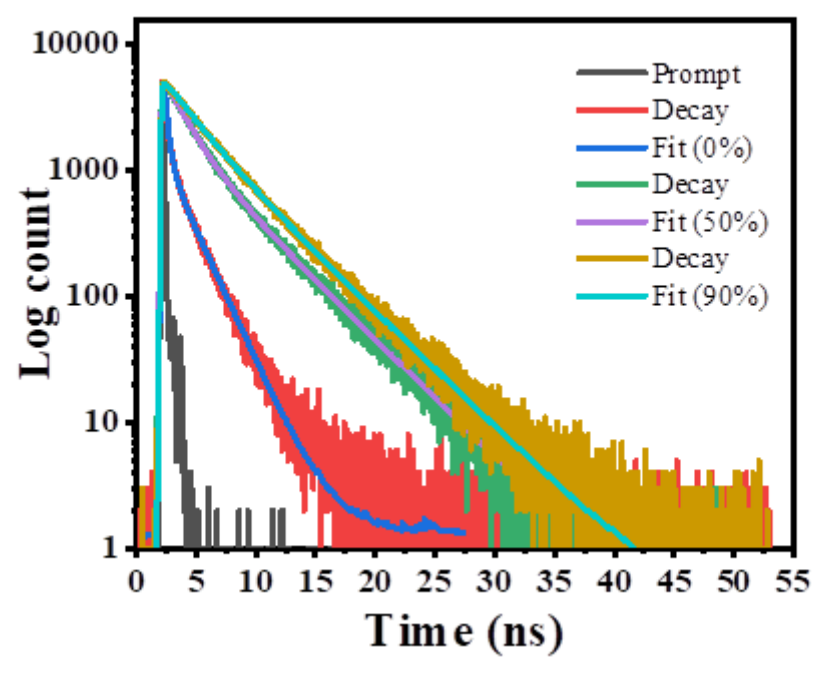


Figure 17. TCSPC graph of L-ArgPy when aggregated with MeOH-H₂O mixture.

AIE active molecules were excited with a 371 nm laser. The excitedstate lifetime decay was fitted by using multiexponential decay and defined as.

$$I(t) = \sum \alpha_i \exp\left(-\frac{t}{\tau_i}\right)$$

Here, τ_i and α_i are the lifetime and amplitude, respectively. The average lifetime can be calculated as

$$\langle \tau_i \rangle = \frac{\sum \alpha_i \, \tau_i}{\sum \alpha_i}$$

The best data fitting was done by maintaining the c2 value approximately unity in all the cases

Table 1. TCSPC Table of L-ArgPy when aggregated with MeOH-H₂0 mixture.

MeOH-Water	Emission (nm)	A1	T1 (ns)	A2	T2 (ns)	Life time (ns)	CHISQ
Fw = 0% (Exc = 371 nm)	420	0.85	0.27932	0.15	0.20708	0.5462555	1.214233
Fw = 50% (Exc = 371 nm)	445	0.65	1.7361	0.35	4.6558	2.76031	1.135953
Fw = 90% (Exc = 371 nm)	505	0.43	2.4183	0.57	4.7496	3.75329	1.098785

In the above table, the TCSPC (Time-Correlated Single Photon Counting) data for L-ArgPy are investigated at fw = 0%, 50%, and 90% in MeOH-H2O mixture, using an excitation wavelength of 371 nm. The fluorescence lifetimes increase noticeably across these samples, from **0.546 ns** in pure methanol to **2.760 ns** in 50% water, and further to **3.753 ns** in 90% water in a methanol-water mixture.

Since a longer fluorescence lifetime indicates that the excited state is less susceptible to quenching and the molecule remains excited longer before returning to the ground state, it has more time to emit fluorescence. This typically leads to stronger fluorescence intensity.

The steady increase in lifetime with increasing water content strongly supports the occurrence of aggregation-induced emission (AIE). As water is added, *L-ArgPy* undergoes aggregation, which restricts non-radiative decay pathways such as vibrational and rotational relaxation.

This suppression of non-radiative losses results in longer lifetimes and enhanced fluorescence emission, confirming the role of aggregation in modulating photophysical behavior.

5.4. Quantum yield Calculation:

The quantum yield measurement was done using the reference quinine sulfate (ϕ =0.54) with the exciting wavelength at 360 nm. The quantum yield was calculated by using the formula:

$$\phi_{samp} = \phi_{stand} \frac{F_{samp}}{F_{stand}} \frac{f_{stand}}{f_{samp}} \left(\frac{\eta_{samp}}{\eta_{stand}} \right)^{2}$$

Where, F_{samp} and F_{stand} = integrated fluorescence intensity, f_{samp} and f_{stand} = absorbance factor, f_{samp} and f_{stand} = fluorescence quantum yield of sample and standard, respectively. h_{samp} and h_{stand} = refractive indices of the sample and standard, respectively.

Table 2. For quantum yield, and radiative, non-radiative, and electron transfer rate constant of L-ArgPy in MeOH-H₂O mixture.

L-ArgPy	τ (ns)	ф(%)	$k_r (10^8 s^{-1})$	$k_{nr}(10^8 \text{ s}^{-1})$	k _{et} (ns)
$f_{w}=0\%$	0.546	8.9	1.630	1.668	35.357
$f_w = 50\%$	2.7603	39	1.412	0.220	0.362
$f_{w} = 90\%$	3.753	48.6	1.294	0.136	0.211

Herein, we calculated quantum yield of L-ArgPy in MeOH-H2O solvent mixture as determined by quinine sulfate as the standard reference and maintaining the absorption less than 1. The quantum yield of L-ArgPy are 8.9% in pure methanol, and it increased to 39% and 48.6% as the water content increases to 50% and 90% in MeOH-H2O mixture. Stronger fluorescence emission is directly correlated with a larger quantum yield, which is known as the ratio of photons emitted to photons absorbed. This pattern implies that when the water content rises, aggregation-induced emission (AIE) takes place. The non-radiative

decay rate constants, which drop dramatically from 35.357 to 0.362 and subsequently to 0.211, also help us comprehend this.

5.5. Morphological and Mechanistic Study:

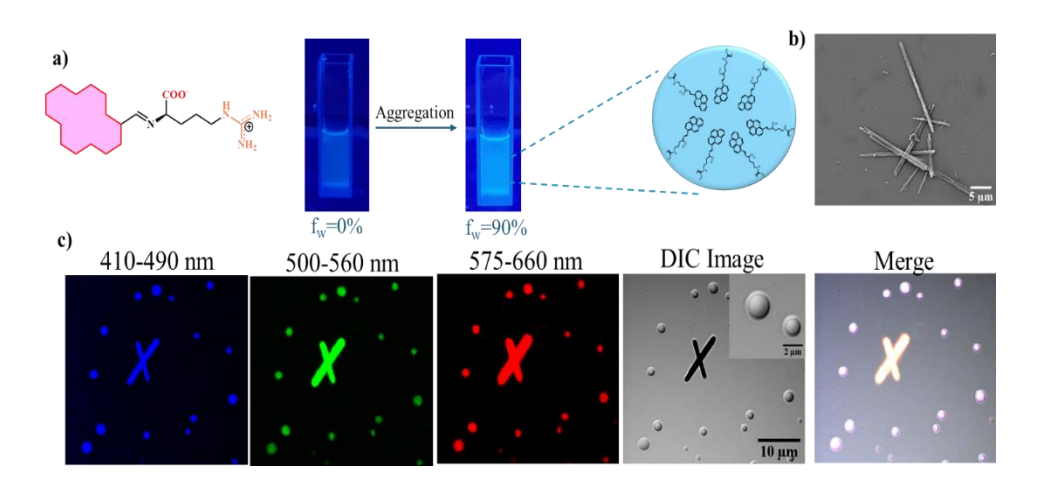


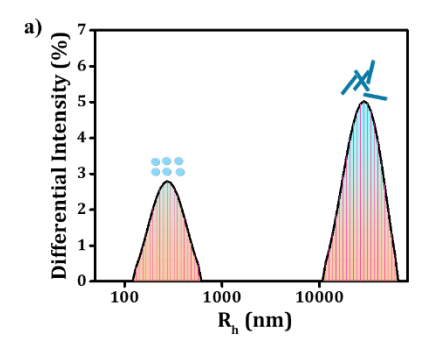
Figure 18. a) LLPS behavior of L-ArgPy in a MeOH–water mixture (90% v/v) upon aggregation, **b)** FE-SEM image of L-ArgPy in MeOH–water (90% v/v) taken after 40 hours, **c)** Confocal image of L-ArgPy in MeOH–water (90% v/v)

As seen in **Figure 18.a**), the molecular structure of L-ArgPy is shown alongside image under UV light (365 nm) of the L-ArgPy in pure methanol solution and in a 90% water—methanol mixture. It is evident from the images that the addition of water induces aggregation. This aggregation restricts non-radiative decay pathways, resulting in enhanced fluorescence i.e., aggregation-induced emission (AIE). The increased fluorescence intensity in the 90% water in MeOH-H2O mixture, compared to the 0% water sample, clearly supports this observation.

In **Figure 18.b**), the **FE-SEM image** provides high-resolution morphological evidence of the final aggregated state of the 90% water sample of L-ArgPy, taken 40 hours after aggregation.

Furthermore, we did the confocal microscopy of L-ArgPy at fw = 90% in MeOH-H2O mixture is shown in Figure 21c, taken 24 hours after aggregation found rod-like structure as well as liquid droplets. It reveals the formation of aggregated structures, indicating supramolecular self-

assembly likely proceeding via liquid–liquid phase separation (LLPS). Over time, this results in the development of a rod-shaped morphology. These findings suggest that the observed aggregation-induced emission arises due to coacervation-induced emission, essentially, the formation of coacervate-like liquid droplets drives the self-assembly and enhances fluorescence.



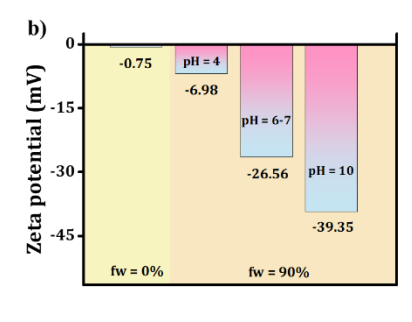


Figure 19. a) Hydrodynamic diameter and particle size distribution of the L-ArgPy in a MeOH-water mixture (10:90 v/v), (20ul from a 1mg/ml mixture). **B)** Zeta potential of the L-ArgPy aggregated at fw =0 and 90% in MeOH-H2O mixture (at pH 4,7 and 10, respectively).

In **Figure 19 a)**, the DLS (Dynamic Light Scattering) graph for L-ArgPy is shown. It displays two distinct size distributions: the smaller size corresponds to liquid droplets formed during LLPS (liquid–liquid phase separation) following aggregation, while the larger size corresponds to rod-like structures that evolve from these droplets over time.

Figure 19 b) presents the zeta potential measurements of L-ArgPy. In pure methanol, the zeta potential is recorded as -0.75 mV. This nearneutral value suggests that L-ArgPy exists predominantly in a zwitterionic form under these conditions. However, in the aggregated state (at 90% water) at different pH values (pH 4, 7, and 10), the zeta potentials are -6.98 mV, -26.56 mV, and -39.35 mV, respectively.

At neutral pH (6-7), aggregation leads to the formation of liquid droplets or coacervate-like structures. In these assemblies, the carboxylate (– COO[–]) groups are oriented toward the droplet surface, while the hydrophobic pyrene moieties are buried inside, away from the aqueous environment, resembling micelle-like organization. This surface excess of negatively charged groups explains the significantly negative zeta potential of –26.56 mV.

At basic pH (10), additional deprotonation occurs, including deprotonation of both carboxylic and even guanidinium groups, resulting in an increased net negative surface charge. This is reflected in the even more negative zeta potential of -39.35 mV. Conversely, at acidic pH (4), the carboxylic acid groups are mostly protonated and not ionized (i.e., not in the –COO⁻ form), leading to a reduction in surface charge. This is supported by the observed zeta potential of –6.98 mV.

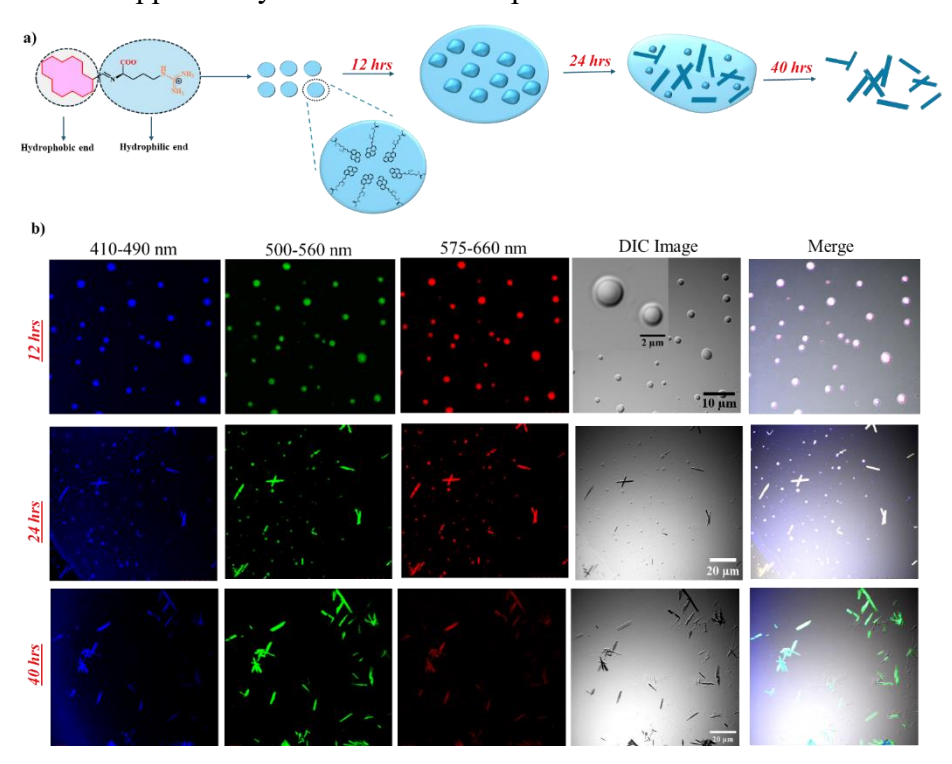


Figure 20. a) Proposed mechanism of aggregation of L-ArgPy in a MeOH—water mixture (90% v/v water). **b)** Confocal microscopy images of L-ArgPy recorded at different time intervals - 12 h, 24 h, and 40 h- show the progression of aggregation and morphological evolution.

In the above Figure, a schematic representation of the aggregation process of L-ArgPy is shown. As illustrated in Figure 20 a. The molecule consists of a hydrophobic segment (pyrene moiety) and a hydrophilic segment (arginine). Upon the addition of water, aggregation is triggered via liquid–liquid phase separation (LLPS), resulting in the formation of coacervate-like droplets. In these spherical droplets, the hydrophobic pyrene units are directed toward the interior, while the hydrophilic arginine groups orient toward the aqueous surface, a configuration driven primarily by electrostatic interactions and hydrophobic effects.

Over time, particularly after 24 hours, these initial droplets come into closer proximity, allowing the pyrene units to interact through π – π stacking. This leads to a more ordered supramolecular self-assembly, resulting in the formation of rod-like structures.

This two-step aggregation mechanism from LLPS-mediated droplet formation to anisotropic rod-like assembly is further supported by the confocal microscopy images captured at different time intervals, as shown in Figure 20 b.

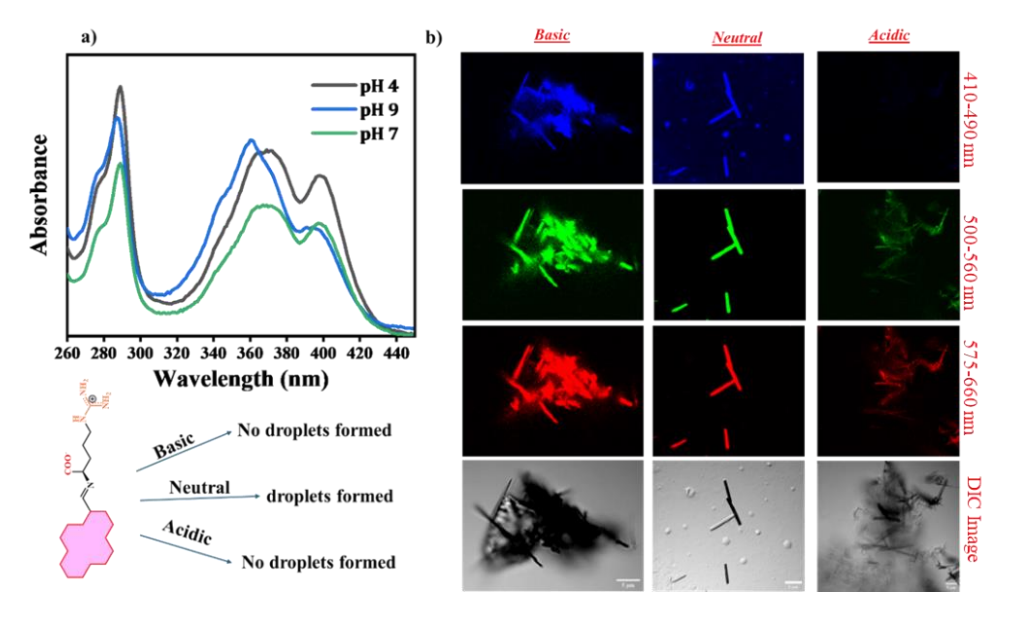


Figure 21 a) UV–Visible absorption spectra of L-ArgPy in MeOH after aggregation with 90% (v/v) water at different pH conditions -acidic (pH 4), neutral (pH 7), and basic (pH 9), along with a schematic representation of the proposed aggregation mechanism under these pH environments. **b)** Confocal

microscopy images of L-ArgPy under basic, neutral, and acidic conditions, respectively.

Figure 21 a) shows the UV–Visible absorption spectra of L-ArgPy at different pH values -pH 4 (acidic), pH 7 (neutral), and pH 9 (basic). The spectral variations under these conditions indicate that the molecular environment and electronic interactions of L-ArgPy are pH-dependent. Changes in the absorption features suggest that the extent of π – π stacking and possible aggregation behaviour is influenced by the protonation state of functional groups, which varies across acidic, neutral, and basic conditions.

In Figure 21 b, confocal microscopy images of L-ArgPy under the same pH conditions are presented. These images confirm that distinct droplet-like structures are observed only at neutral pH, whereas such assemblies are absent in both acidic and basic environments. This supports the interpretation that L-ArgPy undergoes LLPS and forms coacervate-like droplets specifically under neutral conditions, where the balance of hydrophilic and hydrophobic interactions appears to favor phase separation and supramolecular organization.

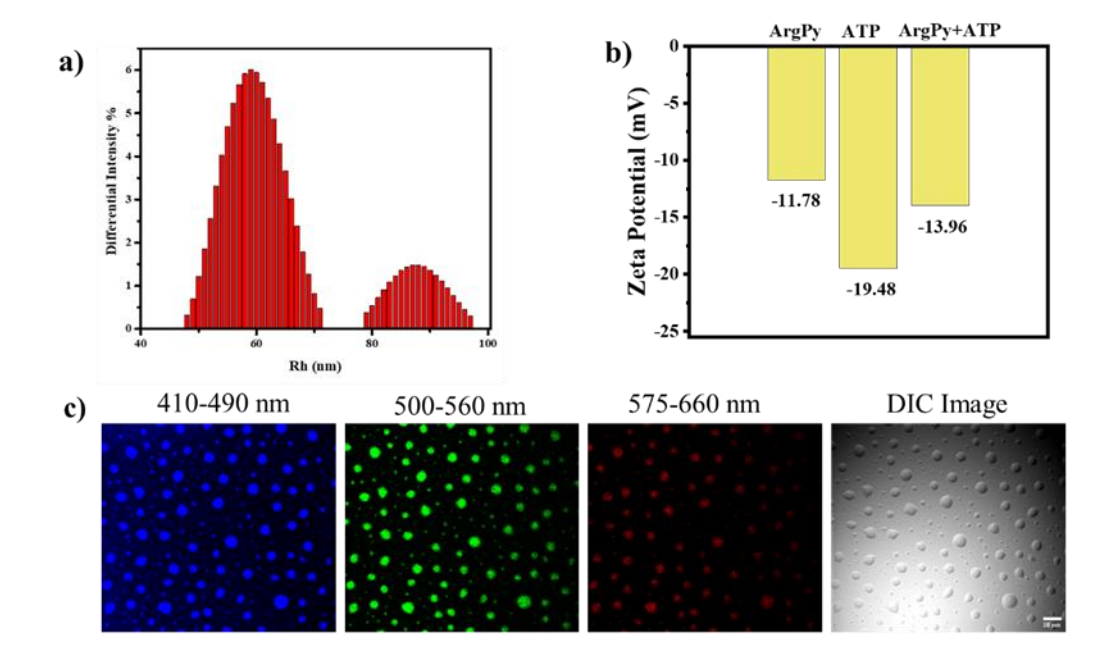


Figure 22. a) DLS profile of L-ArgPy in a DMSO-water mixture (90% v/v), **b)** Zeta potential measurements of L-ArgPy in DMSO-water (90% v/v), ATP, and the L-ArgPy + ATP complex, **c)** Confocal image of L-ArgPy in DMSO-water (90% v/v) acquired 12 hours post-aggregation.

In Figure 22.a), the DLS data of L-ArgPy in a DMSO–Water mixture (fw = 90% v/v) show two distinct size distributions. The smaller peak corresponds to liquid droplet-like structures, while the larger peak is attributed to rod-like aggregates, indicating a transition from initial LLPS to ordered supramolecular assembly. On the other hand, we designed the AIE-active molecule L-ArgPy with potential theranostic applications in mind. L-ArgPy contains a guanidinium group, which is known to interact with negatively charged species such as phosphate, sulfate, and carboxylate ions. Since bacterial cell surfaces are negatively charged, L-ArgPy is expected to interact effectively with them through electrostatic attraction. To investigate this interaction, we studied the binding between the guanidinium group of L-ArgPy and ATP by measuring zeta potential. As shown in Figure 22 b), the zeta potential of aggregated L-ArgPy (fw = 90%) was -11.78 mV, while ATP showed

a value of –19.48 mV. The mixture of L-ArgPy and ATP exhibited an intermediate zeta potential of –13.96 mV, suggesting an interaction between the guanidinium groups of L-ArgPy and the phosphate groups of ATP. Finally, confocal microscopy imaging (**Figure 24c**) of L-ArgPy in the DMSO–water mixture confirmed the formation of droplet-like assemblies, supporting the occurrence of LLPS-driven aggregation in this system.

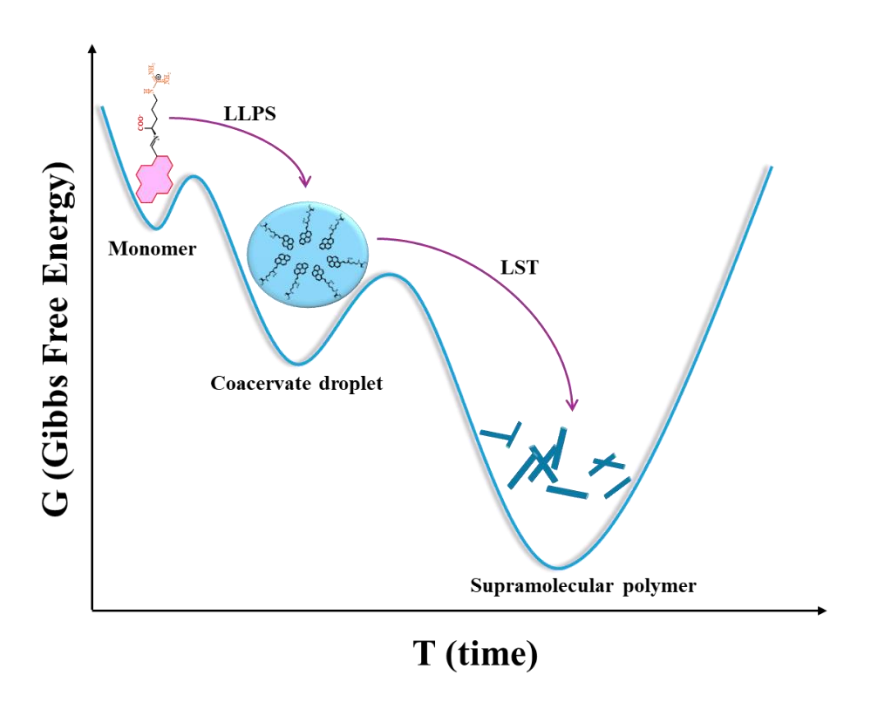


Figure 23. Schematic representation of the proposed synthetic approach, where coacervate droplets are formed via liquid–liquid phase separation (LLPS) of L-ArgPy, enabling controlled supramolecular polymerization.

In the above figure, a schematic representation of the proposed LLPS-driven aggregation mechanism of L-ArgPy is illustrated upon mixing with a methanol-water solvent mixture. The figure highlights the formation of metastable liquid droplets, or coacervate-like structures, which serve as a dormant reservoir of monomers. These droplets allow for a controlled and time-dependent supramolecular polymerization, eventually leading to the formation of ordered assemblies. This mechanism emphasizes the role of LLPS not only in phase separation

but also in regulating the dynamics of supramolecular self-assembly in aqueous environments.

Chapter 6: Dual Emissive nature of L-ArgPy

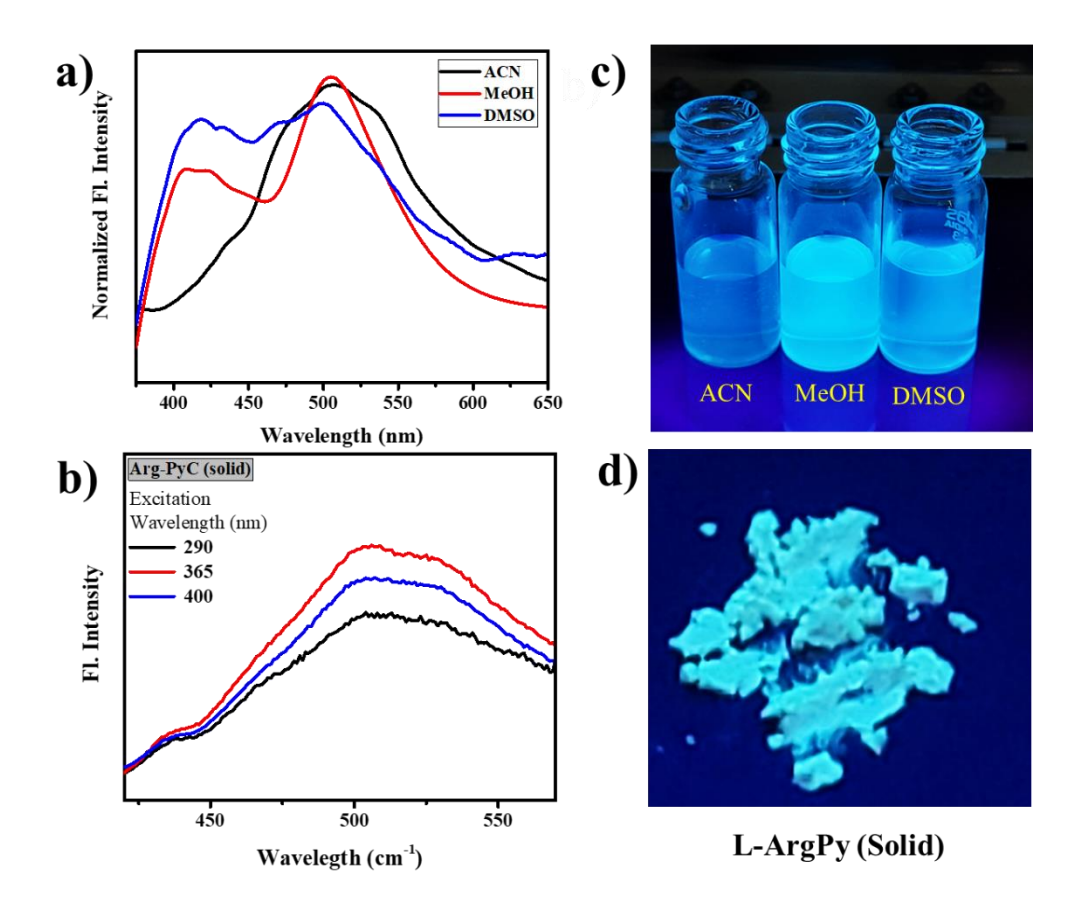


Figure 24. a) FL intensity spectrum (λ_{Exc} =365nm), b) Photographs (under UV light) of L-ArgPy in various solvents, c) FL (solid-state) intensity spectrum of the L-ArgPy and d) Photograph of L-ArgPy under UV light.

As shown above, the fluorescence spectra of L-ArgPy were measured in three different solvents: methanol (MeOH), acetonitrile (ACN), and dimethyl sulfoxide (DMSO), as well as for the solid-state compound. In MeOH and DMSO, two distinct peaks were observed: the first around 450 nm, which is assumed to be from photoinduced electron transfer (PET) from the monomeric species, and the second at 505 nm, is taken to correspond to emission from dimeric species formed via stable ground-state aggregation. In ACN, only a single peak was observed at 505 nm, indicating dominant dimer formation. The absence of the PET peak in ACN suggests that the charge-separated state

required for PET needs to be stabilized effectively in this polar aprotic solvent.

The fluorescence spectrum appeared broad at 505 nm in the solid state, characteristic of aggregated dimeric species or excimer-like interactions. This broad emission indicates multiple emissive states within the aggregated dimer, likely caused by variations in intermolecular interactions or conformational heterogeneity in the solid state. Notably, no emission attributable to PET was observed in the solid state, confirming the exclusive presence of aggregated species

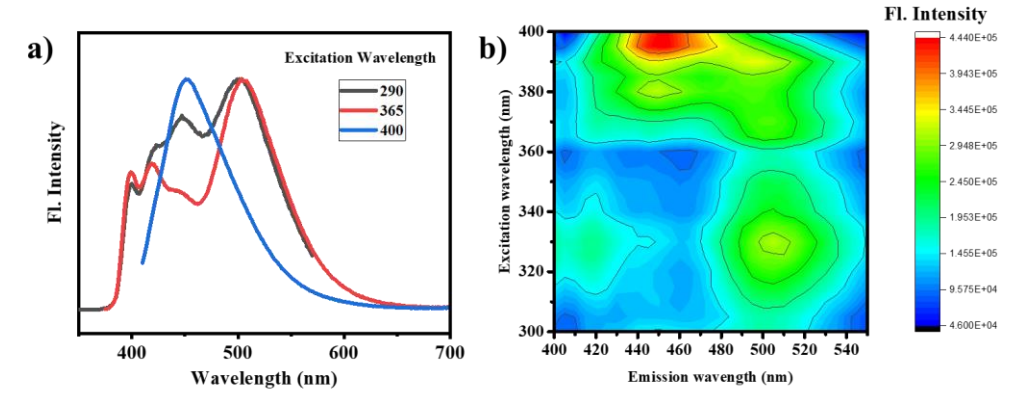


Figure 25. a) Emission spectrum of L-ArgPy in MeOH at different excitation wavelengths (290 nm,365 nm, and 400 nm), respectively, **b)** 3-D spectra (contour view) of L-ArgPy in MeOH.

As shown above, the fluorescence spectra of L-ArgPy were measured in MeOH-Water Mixture (80%, v/v) at different excitation wavelengths. Also, 3-D spectra were taken at excitation wavelengths ranging from 300-400 nm. A single peak was obtained, which is assumed to be due to PET when excited at 400 nm, while for excitations at 365 nm and 290 nm, along with PET peaks, a peak at 505nm was also observed, which is assumed to be due to the presence of dimer in the ground state. This can also be confirmed by looking at the 3-D Spectra of the compound.

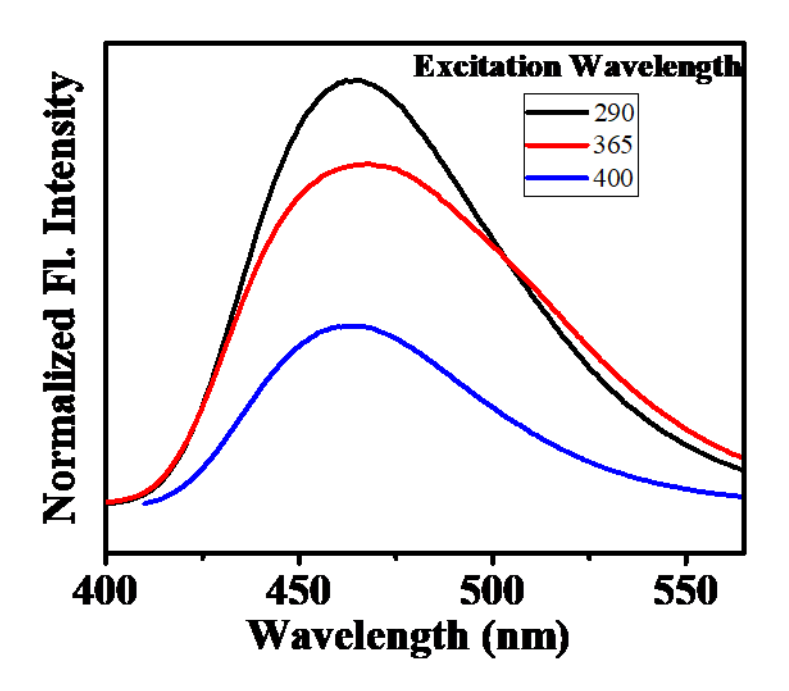


Figure 26. The emission spectrum of L-ArgPy in MeOH-Water (50% v/v) at different excitation wavelengths (290 nm, 365 nm, and 400 nm), respectively.

The fluorescence spectra of the MeOH-water (50%) mixture at excitation wavelengths of 290 nm, 365 nm, and 400 nm exhibited a consistent emission peak around 450 nm. The presence of 50% water in the solvent mixture increased the effective polarity, influencing the fluorescence behavior by stabilizing the emission peak. This highlights the solvent polarity's role in shaping the compound's photophysical properties under these conditions.

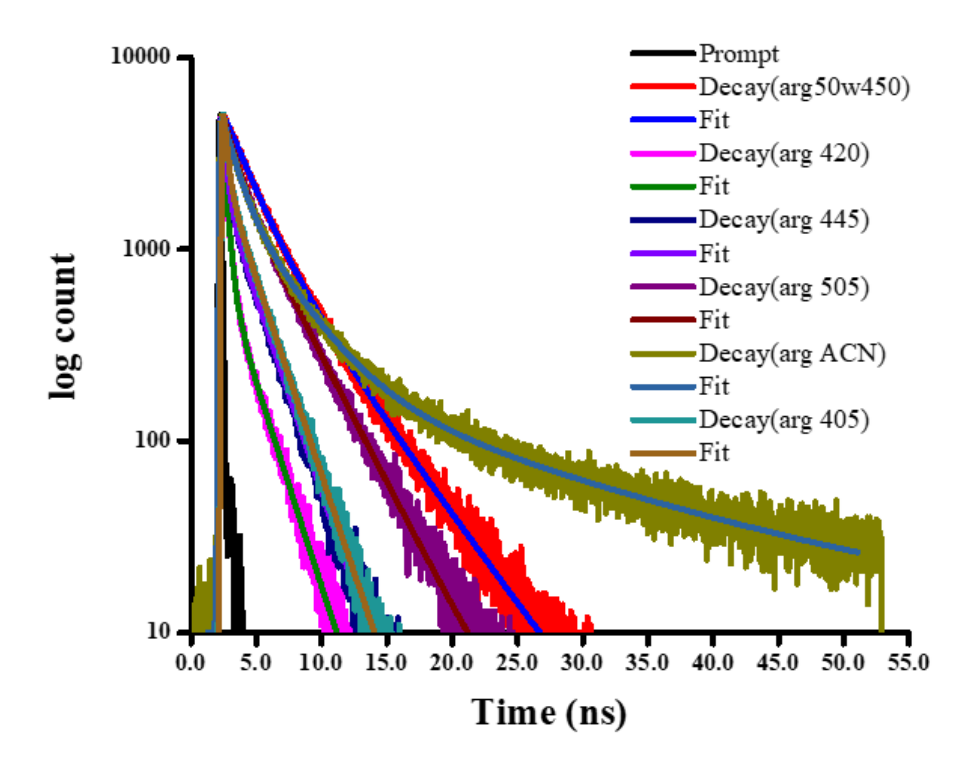


Figure. 27. TCSPC study of L-ArgPy in MeOH and ACN.

Table 3. TCSPC Table of L-ArgPy in MeOH and ACN.

MeOH-W	ater		nission m)	A1		T1 (ns)		A2		T2 (ns)	Life time (ns)	CHISQ
Fw = 0%	Exc = 371 nr	n) 42	0	0.91		0.4624604		0.09		1.849842	0.443	1.145077
Fw = 0%	w = 0% (Exc = 371 nm) 445		5	0.76		0.7442189		0.24	0.24 2.97		0.755	1.079033
Fw = 0%	Exc = 371 nr	n) 50	5	0.51		1.327162		0.49		5.30865	2.097	1.234074
Fw = 0%	Exc = 405 nr	n) 45	0	0.69		0.306018	6	0.31		2.114052	0.865	1.094888
Fw = 50%	(Exc = 371 r	m) 45	0	0.67		2.006318		0.33		4.624009	2.863	1.035116
ACN	Postorton	A 1	TP1 ()	4.0	то	(Α.		Tre) (·)	7 10 dina	CHICO
ACN (Exc = 371 nm)	Emission (nm)	A1	T1 (ns)	A2	12	(ns)	A	•	13	3 (ns)	Life time (ns)	CHISQ
Fw = 0%	505	0.38	3.462744	0.58	0.9	9486882	0.0	04	18	.21736	2.569	1.064415

As shown above, a TCSPC Study was performed for the L-ArgPy compound in MeOH and DMSO solvents. The time-resolved fluorescence studies of L-ArgPy using TCSPC provided critical insights into the photophysical behaviour of the compound in different

environments. In methanol (MeOH), two distinct lifetime ranges were observed; it was assumed that (~0.443–0.755 ns) corresponded to the PET emission and (~2.097 ns) corresponded to the dimer emission.

Based on current Experiments and previously reported data, the shorter lifetime is assumed to be associated with the charge-separated state formed during PET. The longer lifetime indicates a stable excited state in the aggregated dimeric species. In acetonitrile (ACN), only a single lifetime (~2.569 ns) at 505nm was detected, consistent with the exclusive presence of dimeric species; PET is suppressed due to insufficient stabilization of the charge-separated state in this polar aprotic solvent.

Chapter 7: Future scope of work

- 1) Extended Solvent Study for L-ArgPy.
- 2) Morphological study for dual emission.
- 3) Application Studies:
 - Antibacterial study.
 - Explore practical applications of dual-emission peaks for advanced ratio metric sensing, particularly in bio-sensing and environmental monitoring.

Chapter 8: Conclusion

1) Research Objective:

- Designed and synthesized an amino acid-derived Aggregation-Induced Emission (AIE) active molecule for potential biological and soft material applications.
- Emphasis on developing a non-toxic, biocompatible system with tunable photophysical properties and self-assembly behavior.

2) Significant Findings

- Successful synthesis of L-ArgPy, a pyrene—arginine Schiff base, under mild and neutral conditions.
- Structural confirmation achieved through FT-IR, LC-MS, and NMR spectroscopy

3) Photophysical Properties:

- L-ArgPy exhibited classic AIE behaviour in DMSO-water and MeOH-water solvent mixtures.
- Displayed dual emission peaks, suggesting the presence of both monomeric and excimer states.
- Fluorescence lifetime studies indicated excitation- and concentration-dependent decay behaviour, supporting the dynamic nature of its emissive states.

4) Morphological and Mechanistic Analysis:

- Aggregation of L-ArgPy was found to proceed through liquid liquid phase separation (LLPS), forming coacervate-like droplets.
- These droplets subsequently underwent π-π stacking-driven supramolecular polymerization, resulting in anisotropic rodlike nanostructures, as observed via microscopy.

• This bioinspired self-assembly pathway mimics LLPS-to-Fiber transitions found in biological systems.

5) Biological and Functional Applications:

- Preliminary testing revealed **antibacterial activity** of L-ArgPy against common microbial strains.
- Fluorescence quenching experiments indicated promising biosensing ability toward *E. coli*, suggesting potential as a turn-off fluorescent sensor for bacterial detection.

Chapter 9: References

- (1) Zhu, C.; Kwok, R. T. K.; Lam, J. W. Y.; Tang, B. Z. Aggregation-Induced Emission: A Trailblazing Journey to the Field of Biomedicine. *ACS Appl. Bio Mater.* **2018**, *1* (6), 1768–1786. https://doi.org/10.1021/acsabm.8b00600.
- (2) Hong, Y.; Lam, J. W. Y.; Tang, B. Z. Aggregation-Induced Emission. *Chem. Soc. Rev.* **2011**, *40* (11), 5361–5388. https://doi.org/10.1039/C1CS15113D.
- (3) Han, M.; Hara, M. Intense Fluorescence from Light-Driven Self-Assembled Aggregates of Nonionic Azobenzene Derivative. *Journal of the American Chemical Society* **2005**, 127 (31), 10951–10955. https://doi.org/10.1021/ja0509275.
- (4) Li, Y.; Xu, L.; Su, B. Aggregation Induced Emission for the Recognition of Latent Fingerprints. *Chem. Commun.* **2012**, *48* (34), 4109–4111. https://doi.org/10.1039/C2CC30553D.
- (5) Hong, Y.; Lam, J. W. Y.; Tang, B. Z. Aggregation-Induced Emission. *Chem. Soc. Rev.* **2011**, *40* (11), 5361–5388. https://doi.org/10.1039/C1CS15113D.
- (6) Hu, F.; Xu, S.; Liu, B. Photosensitizers with Aggregation-Induced Emission: Materials and Biomedical Applications. *Adv. Mater.* **2018**, *30* (45), 1801350. https://doi.org/10.1002/adma.201801350.
- (7) Luo, J.; Xie, Z.; Lam, J. W. Y.; Cheng, L.; Chen, H.; Qiu, C.; Kwok, H. S.; Zhan, X.; Liu, Y.; Zhu, D.; Tang, B. Z. Aggregation-Induced Emission of 1-Methyl-1,2,3,4,5-Pentaphenylsilole. *Chem. Commun.* **2001**, No. 18, 1740–1741. https://doi.org/10.1039/B105159H.
- (8) Guan, J.; Shen, C.; Peng, J.; Zheng, J. What Leads to Aggregation-Induced Emission? *J. Phys. Chem. Lett.* **2021**, *12* (17), 4218–4226. https://doi.org/10.1021/acs.jpclett.0c03861.
- (9) Wu, W.; Liu, B. Aggregation-Induced Emission: Challenges and Opportunities. *Natl. Sci. Rev.* **2020**, 8 (6), nwaa222. https://doi.org/10.1093/nsr/nwaa222.

- (10) Hong, Y.; Lam, J. W. Y.; Tang, B. Z. Aggregation-Induced Emission: Phenomenon, Mechanism and Applications. *Chem. Commun.* **2009**, No. 29, 4332–4353. https://doi.org/10.1039/B904665H.
- (11) Liu, X.; Liang, G. Dual Aggregation-Induced Emission for Enhanced Fluorescence Sensing of Furin Activity in Vitro and in Living Cells. *Chem. Commun.* **2017**, *53* (6), 1037–1040. https://doi.org/10.1039/C6CC09106G.
- (12) Feng, X.; Qi, C.; Feng, H.-T.; Zhao, Z.; Sung, H. H. Y.; Williams, I. D.; Kwok, R. T. K.; Lam, J. W. Y.; Qin, A.; Tang, B. Z. Dual Fluorescence of Tetraphenylethylene-Substituted Pyrenes with Aggregation-Induced Emission Characteristics for White-Light Emission. *Chem. Sci.* **2018**, *9* (25), 5679–5687. https://doi.org/10.1039/C8SC01709C.
- (13) Goswami, N.; Yao, Q.; Luo, Z.; Li, J.; Chen, T.; Xie, J. Luminescent Metal Nanoclusters with Aggregation-Induced Emission. The Journal of Physical Chemistry Letters 2016, 7 (6), 962–975. https://doi.org/10.1021/acs.jpclett.5b02765.
- (14) Wang, C.; Zhao, X.; Wu, K.; Lv, S.; Zhu, C. A Ratiometric Organic Fluorescent Nanogel Thermometer for Highly Sensitive Temperature Sensing. *Biosensors* **2022**, *12* (9), 702. https://doi.org/10.3390/bios12090702.
- (15) Tang, Y.; Zhang, J.; Xiong, Q.; Xie, G.; Jin, S.; Zheng, J.; Rong, R.; Liu, Q.; Zhang, S.; Tao, D.; Jin, F. Fluorescence property and multifaceted applications of an aggregation-induced emission organic small molecule multifunctional material. *Journal of Luminescence* **2025**, 121202. https://doi.org/10.1016/j.jlumin.2025.121202.
- (16) Yu, J.; Zhao, X.; Han, L.; Miao, J.; Guo, J.; Li, B.; Zhang, Z.; Wu, Y.; Wang, X.; Chen, L. Encapsulation Strategy Based on Aggregation-Induced Emission Effect for the Dual-Emission Ratiometric Fluorescence Detection of Tetracycline. *Talanta* **2025**, *293*, 128107. https://doi.org/10.1016/j.talanta.2025.128107.
- (17) Patra, S.; Sharma, B.; George, S. J. Programmable coacervate droplets via Reaction-Coupled Liquid–Liquid Phase separation (LLPS)

- and competitive inhibition. *Journal of the American Chemical Society* **2025**. https://doi.org/10.1021/jacs.4c17063.
- (18) *X-MOL*. x-mol.net. https://www.x-mol.net/paper/article/5742271.
- (19) Yewdall, N. A.; André, A. A. M.; Lu, T.; Spruijt, E. Coacervates as models of membraneless organelles. Current Opinion in Colloid & Interface Science 2020, 52, 101416. https://doi.org/10.1016/j.cocis.2020.101416.
- (20) Yewdall, N. A.; André, A. A. M.; Lu, T.; Spruijt, E. Coacervates as Models of Membraneless Organelles. *Curr. Opin. Colloid Interface Sci.* **2021**, *52*, 101416. https://doi.org/10.1016/j.cocis.2020.101416.
- (21) Yang, S.; Yu, H.; Xu, X.; Yang, T.; Wei, Y.; Zan, R.; Zhang, X.; Ma, Q.; Shum, H. C.; Song, Y. AIEgen-Conjugated Phase-Separating Peptides Illuminate Intracellular RNA through Coacervation-Induced Emission. *ACS Nano* **2023**, *17* (9), 8195–8203. https://doi.org/10.1021/acsnano.2c12072.
- (22) Abbas, M.; Lipiński, W. P.; Wang, J.; Spruijt, E. Peptide-Based Coacervates as Biomimetic Protocells. *Chem. Soc. Rev.* **2021**, *50* (6), 3690–3705. https://doi.org/10.1039/D0CS00307G.
- (23) Brangwynne, C. P.; Eckmann, C. R.; Courson, D. S.; Rybarska, A.; Hoege, C.; Gharakhani, J.; Jülicher, F.; Hyman, A. A. Germline P granules are liquid droplets that localize by controlled Dissolution/Condensation. *Science* **2009**, 324 (5935), 1729–1732. https://doi.org/10.1126/science.1172046.
- (24) Patra, S.; Chandrabhas, S.; Dhiman, S.; George, S. J. Controlled Supramolecular Polymerization via Bioinspired, Liquid–Liquid Phase Separation of Monomers. *J. Am. Chem. Soc.* **2024**, *146* (18), 12577–12586. https://doi.org/10.1021/jacs.4c01377.
- (25) Patra, S.; Chandrabhas, S.; J. George, S. Bioinspired Programmable Coacervate Droplets and Self-Assembled Fibers through pH Regulation of Monomers. *J. Mater. Chem. B* **2025**, *13* (2), 604–609. https://doi.org/10.1039/D4TB01550A.

- (26) Zou, Q.; Yan, X. Amino Acid Coordinated Self-Assembly. *Chem. Eur. J.* **2018**, *24* (4), 755–761. https://doi.org/10.1002/chem.201704032.
- (27) Ren, H.; Wu, L.; Tan, L.; Bao, Y.; Ma, Y.; Jin, Y.; Zou, Q. Self-Assembly of Amino Acids toward Functional Biomaterials. *Beilstein J. Nanotechnol.* **2021**, *12*, 1140–1150. https://doi.org/10.3762/bjnano.12.85.
- (28) Yang, X.; Lu, H.; Wu, B.; Wang, H. Triggered Self-Sorting of Peptides to Form Higher-Order Assemblies in a Living System. *ACS Nano* **2022**, *16* (11), 18244–18252. https://doi.org/10.1021/acsnano.2c05825.
- (29) Zhu, X.; Chen, X.; Liu, H.; Sun, B. Amino-Acid-Encoded Supramolecular Self-Assembly Architectures: Near-Infrared Fluorescence–Photothermal Temperature Dual-Signal Sensing of Hydrogen Peroxide. *ACS Sustain. Chem. Eng.* **2024**, *12* (12), 4803–4812. https://doi.org/10.1021/acssuschemeng.3c05814.
- (30) Tang, C. W.; VanSlyke, S. A. Organic Electroluminescent Diodes. *Appl. Phys. Lett.* **1987**, *51* (12), 913–915. https://doi.org/10.1063/1.98799.
- (31) La Manna, S.; Di Natale, C.; Onesto, V.; Marasco, D. Self-Assembling Peptides: From Design to Biomedical Applications. *Int. J. Mol. Sci.* **2021**, *22* (23), 12662. https://doi.org/10.3390/ijms222312662.
- (32) Bera, S.; Xue, B.; Rehak, P.; Jacoby, G.; Ji, W.; Shimon, L. J. W.; Beck, R.; Král, P.; Cao, Y.; Gazit, E. Self-Assembly of Aromatic Amino Acid Enantiomers into Supramolecular Materials of High Rigidity. *ACS Nano* **2020**, *14* (2), 1694–1706. https://doi.org/10.1021/acsnano.9b07307.
- (33) Panigrahi, A.; Are, V. N.; Jain, S.; Nayak, D.; Giri, S.; Sarma, T. K. Cationic Organic Nanoaggregates as AIE Luminogens for Wash-Free Imaging of Bacteria and Broad-Spectrum Antimicrobial Application. *ACS Appl. Mater. Interfaces* **2020**, *12* (5), 5389–5402. https://doi.org/10.1021/acsami.9b15629.

- (34) Feng, X.; Wang, X.; Redshaw, C.; Tang, B. Z. Aggregation Behaviour of Pyrene-Based Luminescent Materials, from Molecular Design and Optical Properties to Application. *Chem. Soc. Rev.* **2023**, *52* (19), 6715–6753. https://doi.org/10.1039/D3CS00251A.
- (35) Panigrahi, A.; Sahu, B. P.; Mandani, S.; Nayak, D.; Giri, S.; Sarma, T. K. AIE Active Fluorescent Organic Nanoaggregates for Selective Detection of Phenolic-Nitroaromatic Explosives and Cell Imaging. *J. Photochem. Photobiol. Chem.* **2019**, *374*, 194–205. https://doi.org/10.1016/j.jphotochem.2019.01.029.